Ph.D. Dissertation

Designing 2D-based Electrodes for Intrinsically Stretchable Organic Light-Emitting Diodes with High Efficiency

고효율 고유 신축성 유기 발광 다이오드를 위한 2D 기반의 전극 디자인

February 2023

Graduate School of Engineering
Seoul National University
Materials Science and Engineering

Shin Jung Han

Designing 2D-based Electrodes for Intrinsically Stretchable Organic Light-Emitting Diodes with High Efficiency

Advisor: Tae-Woo Lee

by

Shin Jung Han

A thesis submitted to the Graduate Faculty of Seoul National University in partial fulfillment of the requirements for the Degree of Doctor of Philosophy
Department of Materials Science and Engineering

February 2023

Approved
by

Chair of Advisory Committee Jeong-Yun Sun (Seal)
Vice-Chair of Advisory Committee Tae-Woo Lee (Seal)
Advisory Committee Jaesang Lee (Seal)
Advisory Committee Keehoon Kang (Seal)
Advisory Committee Jin Jeon (Seal)

Abstract

Designing 2D-based Electrodes for Intrinsically Stretchable Organic Light-Emitting Diodes with High Efficiency

Shin Jung Han
Department of Materials Science and Engineering
Graduate School of Engineering
Seoul National University

The emergence of wearable electronics, as an alternative to conventional stationery and hand-held instruments, requires integrated devices to be stretchable to form intimate contact with human skin. Such systems can use on-skin sensors to monitor physiological signals by continuously and in real time, and can directly visualize of signals by seamless incorporation of stretchable displays. However, compared with the realm of on-skin sensors, the development of intrinsically stretchable displays is stagnated. The state-of-the-art stretchable displays consisting of fully stretchable layers normally exhibit the low performance due to the limitations of stretchable electrode characteristics and the absence of a protocol of the lamination process.

The development of intrinsically-stretchable organic light-emitting didoes (ISOLEDs) has stagnated due to the lack of ideal stretchable electrode materials to

overcome the existing issue of poor charge injection at the electrode interface, and consequent high turn-on voltage V_{on} > 7 V, although the stretchability has been improved significantly. Herein, we present a two-dimensional-contact stretchable electrode (TCSE) that consists of AgNWs as the conductive filler, two-dimensional graphene as the work function (*WF*) modifier on the surface, GO binder to enhance conductivity and stretchability, and dopants to control the *WF*. The *WF* of the TCSE can be modulated to 5.69 eV and 4.04 eV by *p*- and *n*-type doping, respectively. TCSE can fulfill the required energy-level alignment with reduced the charge-injection barrier and form a two-dimensional electrical contact with the adjacent organic layer upon lamination for efficient charge injection. An ISOLED using the laminated doped TCSE exhibited low V_{on} of 5.5 V, maximum luminance (L_{max}) of 1130 cd/m^2, current efficiency (CE) of 9.3 cd/A, and a stable light-emission with LT_{50} = 7.07h (the lifetime at 50% initial luminance under continuous operation). Furthermore, we demonstrated a three-inch five-by-five passive matrix ISOLED using the convex stretching method.

To further develop the practical applications of intrinsically stretchable optoelectronic devices with enhanced performances, a new lamination method has been introduced to obtain a uniform lamination contact and strong adhesion at the interface. A minimum operating voltage of intrinsically stretchable organic light-emitting diodes (ISOLEDs) is always required for practical applications. However, the lack of protocols for the lamination makes it extremely challenging to attain a reliable ISOLED without inducing any degradations. Herein, we present a solvent-vapor-assisted lamination (SVAL) method to reinforce the cathode interface, which lowers the operation voltage and increases the stretchability of ISOLEDs. Achieving a uniform contact and strong adhesion at the interface is the key to attaining reliable

lamination. A cold-pressing (CP) treatment was first introduced to reduce the surface roughness of silver nanowires before the embedding process. Subsequent solvent vapor treatment before the lamination partially solvates the surface of the active layer with an increase in the segmental motion of polymer chains, which substantially increases the interfacial adhesion. These benefits from a combination of CP and SVAL considerably reduced threshold voltage V_{th} (i.e., indicates the voltage where current shows an abrupt increase for light-emission) from 6.7 to 2.7 V. The ISOLED also exhibits excellent mechanical stretchability, with no significant change in luminance under 30% strain.

CVD-grown graphene suffers from its poor solution processability and long process time for transferring process, making it less compatible with solution-processed devices. To simplify the process of the two-dimensional contact stretchable electrode, we have introduced MXene as the two-dimensional contact layer for the stretchable AgNW electrode instead of graphene. MXene is a fast-growing material having two-dimensional structure for optoelectronic devices owing to its attractive properties such as *WF* modulating capabilities, metallic conductivity, and solution processability with hydrophilic groups on the surface. Herein we demonstrate MXene-based 2D contact stretchable electrodes for intrinsically stretchable phosphorescent organic light-emitting diodes (ISPhOLEDs). MXenes serve as the 2D interlayer to increase the electrical contact area without sacrificing the stretchability. The *WF* of MCSE can be successfully tuned from 3.79 to 5.71 eV for cathode and anode applications. Besides, we have also proposed a stretchable gradient hole injection layer to facilitate the hole injection with the addition of PFSA. In terms of the light-emitting layer, stretchability can be achieved with the addition of elastomer as the plasticizer. Lastly, the intrinsically stretchable phosphorescent

light-emitting device with the high efficiency has been fabricated for the first time.

This dissertation can provide effective guidelines for designing two-dimensional contactable stretchable electrodes with 2D materials and intrinsically stretchable organic light-emitting diodes with high efficiency.

Keyword: stretchable electrode, silver nanowire, graphene, MXene, solvent-vapor assisted lamination, stretchable GraHIL, stretchable PhEML

Student Number: 2019-34907

Table of Contents

List of Tables

List of Figures

Chapter 1. Introduction

1.1. Development of stretchable displays for wearable electronics

Various wearable electronic devices, including electrical, physical, and chemical sensors that are attachable to the skin, have developed significantly due to recent researches on soft materials and processing technologies **(Figure 1.1)**.[1-4] With the healthcare industry in the spotlight, it is especially important for disease management to guide individuals' exercise and activity, and to check their current body conditions, including heart rate, electrocardiogram, respiratory rate, and muscle conditions.[5-7] These wearable electronic devices require lightness and stretchability to solve the fundamental differences in dynamics between the soft human body and rigid electronic sensors.[8-10] Therefore, wearable electronics need to be stretchable to withstand a variety of mechanical deformation, including bending, twisting, stretching or other complex transformation.

Two strategies can be used to attain the stretching property. One strategy is to apply intrinsically stretchable materials in single or composite designs, and the other is to use specific structures that can go through large deformation without fracture **(Figure 1.2)**.[11] Structural design is an effective approach to assign stretchability to rigid materials, also called a geometric stretchability method.

In particular, out-of-plane buckling is the most widely used technology for applying rigid thin film devices to the complicated surfaces of human skin with wrinkles and waves.[12] First, a thin film is attached to a pre-strained elastomeric substrate, and deformation is restored to form buckling and wave patterns. However,

the stretchable property is largely determined by the thickness of the attached thin film, the degree of the pre-strain, and the adhesive force between the elastomer and the thin film. In addition, these structural designs are difficult to build intimate contact with the human skin.

Hence, the most effective strategy to achieving wearable electronics is to develop intrinsically stretchable materials. In general, the functional device has a multilayer structure such as a substrate, a dielectric, a conductive material, and a semiconductor material. Among them, the conductive polymer can induce phase separation and formation of a stretchable nanofiber structure through micro-structural engineering.[13] In addition, phase separation can achieve a stretchable nanofiber structure even in the conjugated polymer semiconductor and elastomer complex structure.[14] Therefore, this dissertation will focus on the study of organic light-emitting diodes using intrinsically stretchable materials.

Currently, the mechanical properties of stretchable devices have been improved, but research on intrinsically stretchable displays is faced with challenges due to the limitations of the characteristics of high operation voltage and low current efficiency, which are difficult to apply to real applications. The state-of-the-art stretchable display with fully stretchable structures can be strained up to more than 100%, but has the disadvantage of operation under an alternating current field of several kilovolts **(Figure 1.3)**.[5,15-17]

In order to solve this problem, intrinsically stretchable organic light emitting diodes (ISOLEDs) of DC driving with a low operation voltage is preferred for application of wearable electronic devices.[18-23] However, due to conflicting technical problems with the stretchability and operating performance of the device, researches on DC-driven ISOLEDs have not been actively conducted. However, the

reported DC-driven ISOLEDs still show the problem of low current efficiency and high operation voltage due to mismatching of energy level alignment at the interface between the stretchable electrode and the organic semiconductor. An ideal stretchable electrode needs to promote the charge injection capability with work function (*WF*) tunability for improving device characteristics. That is, an electrode having a high *WF* has a superior hole injection performance [24-26], and an electrode having a low *WF* facilitates electron injection capability.[27-29] However, although researches on improving the stretchability of ISOLED are currently progressing [18-23], it is necessary to further develop the characteristics of intrinsically stretchable electrodes that can affect the performance of the device.

Various conductive materials have been used in the researches of stretchable electrodes such as conductive polymers, 1D structured metallic nanowires, and 2D structured graphene and CNTs **(Figure 1.4)**. The electrical and optical properties and mechanical stretchability vary depending on the material. Conventional ISOLEDs with silver nanowire (AgNW) electrodes, a representative conductive material, are difficult to achieve low driving voltage and high current efficiency at the same time **(Figure 1.5)**. However, when the organic light emitting diode has an appropriate band structure, it generally shows excellent device characteristics with high luminance and current efficiency.[24] This result is due to the high charge injection barrier caused by the difference in energy level arrangement between AgNW-based stretchable electrodes and organic interfaces. In addition, the limited electrical contact area between the AgNW network and the charge transport layer may be the cause of the degradation in charge injection capability. That is, in part, because AgNW percolation networks embedded in the elastomeric surface do not form a complete two-dimensional electrode surface, and the *WF* of AgNW is also not

properly modulated. Therefore, it is necessary to improve the performance of ISOLED by facilitating the charge injection capability through the composite electrode structure with a perfect two-dimensional surface and its *WF* modulation.

1.2. Outline of the thesis

In Chapter 2, we propose ISOLEDs with stable charge injection at the electrode interface by designing a two-dimensional-contact stretchable electrode (TCSE) that consists of AgNW percolation network as the conductive filler, two-dimensional graphene as the *WF* modifier exposed to air, GO binder to increase conductivity and stretchability, and dopants to control the *WF*. The *WF* of the TCSE can be tailored from 4.04 to 5.69 eV to fulfill the required energy-level alignment with reduced the charge-injection barrier. Besides, the formation of a two-dimensional continuous electrical contact at the TCSE/organic interface is vital for efficient charge injection, and the ISOLED shows L_{max} = 1130 cd/m^2, V_{on} = 5.5 V, CE = 9.3 cd/A, and a stable light-emission with LT_{50} = 7.07h. Using these tactics, a three-inch five-by-five passive matrix ISOLED also proves the feasibility of the doped TCSE as the electrode and the lamination for large-scale applications.

In Chapter 3, we present a solvent-vapor-assisted lamination (SVAL) method to reinforce the cathode interface, which lowers the operation voltage and increases the stretchability of ISOLEDs. Achieving a uniform contact and strong adhesion at the interface is the key to attaining reliable lamination. A cold-pressing (CP) treatment was first introduced to reduce the surface roughness of silver nanowires before the embedding process. Subsequent solvent vapor treatment before the lamination partially solvates the surface of the active layer with an increase in the segmental

motion of polymer chains, which substantially increases the interfacial adhesion. These benefits from a combination of CP and SVAL reduced threshold voltage V_{th} from 6.7 to 2.7 V. The ISOLED also exhibits excellent mechanical stretchability, with no significant change in luminance under 30% strain. This work will provide a solution to the chronic adhesion problem that occurred at the laminated stretchable cathode interface of ISOLEDs, and will stimulate academic and industrial research on the fundamentals of stretchable optoelectronics for practical applications. To solve the poor solution processability and long processing time for the graphene-based TCSE, MXene has been introduced as a new kind of the two-dimensionally contactable layer.

In Chapter 4, we demonstrate MXene-based 2D contact stretchable electrodes for intrinsically stretchable phosphorescent organic light-emitting diodes (ISPhOLEDs). MXenes serve as the 2D interlayer to increase the electrical contact area without sacrificing the stretchability. The *WF* of MCSE can be successfully tuned from 3.79 to 5.71 eV for cathode and anode applications. Besides, we have also proposed a stretchable gradient hole injection layer to facilitate the hole injection with the addition of PFSA. In terms of the light-emitting layer, stretchability can be achieved with the addition of elastomer as the plasticizer. The intrinsically stretchable phosphorescent light-emitting device has been fabricated for the first time, and this work will provide a guide for designing the solution-processable 2D contact stretchable electrodes and highly efficient light-emitting devices in the future.

This dissertation can provide guidelines for designing two-dimensionally-contactable and stretchable electrodes and intrinsically stretchable organic light-emitting diodes with high efficiency **(Figure 1.6)**.

Figure 1.1 Wearable display for independent wearables. (source: Techtarget.com, Prof. Takao Someya's group)

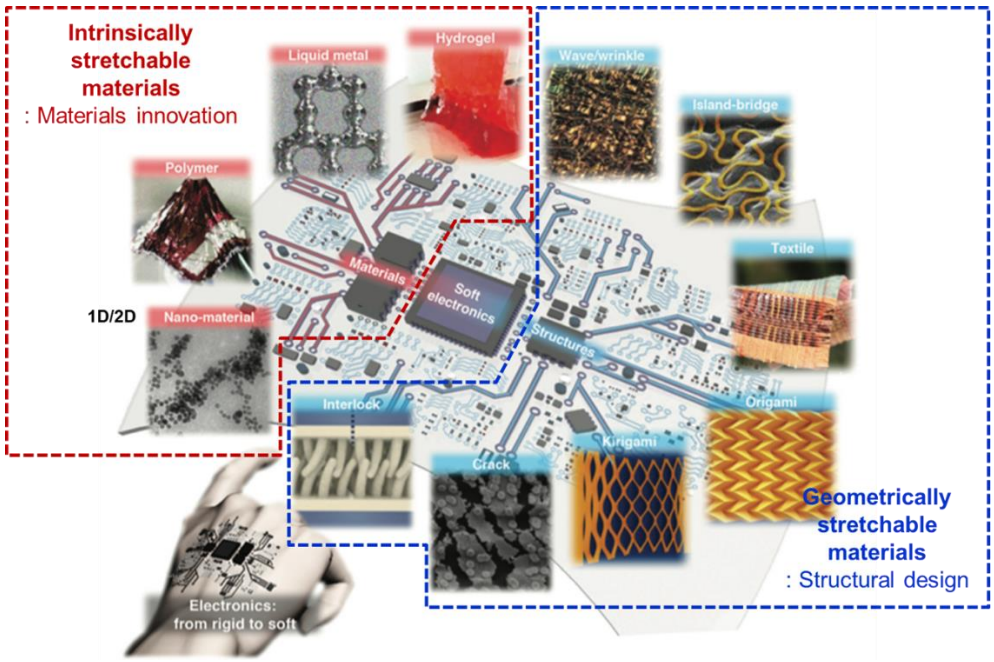

Figure 1.2 Two approaches that can be applied to attain stretchable electronics: 1) stretchable material development, 2) stretchable structure design.[11]

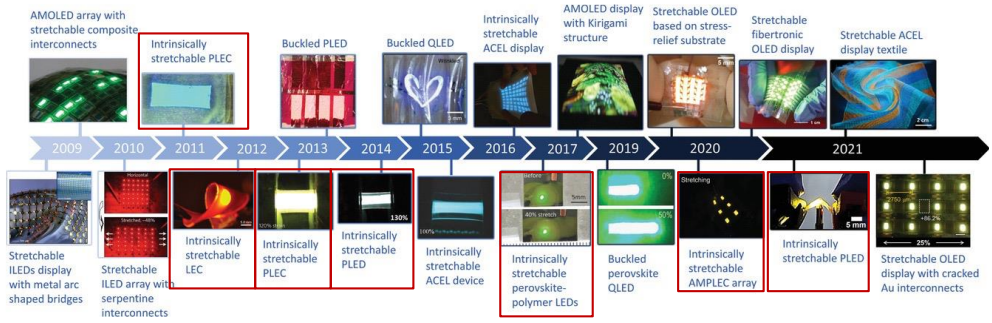

Figure 1.3 Milestones of the research progress of stretchable EL devices.[30]

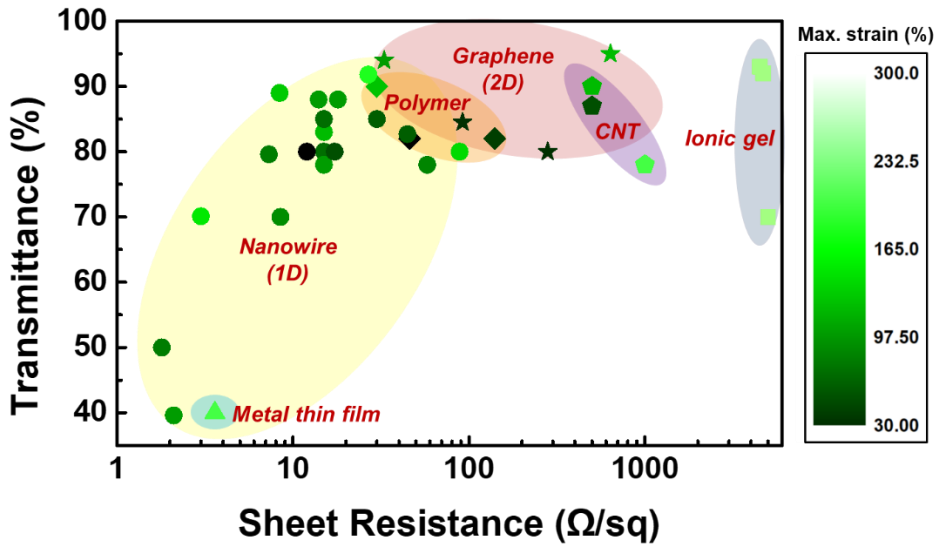

Figure 1.4 Performance of intrinsically stretchable conductive materials.

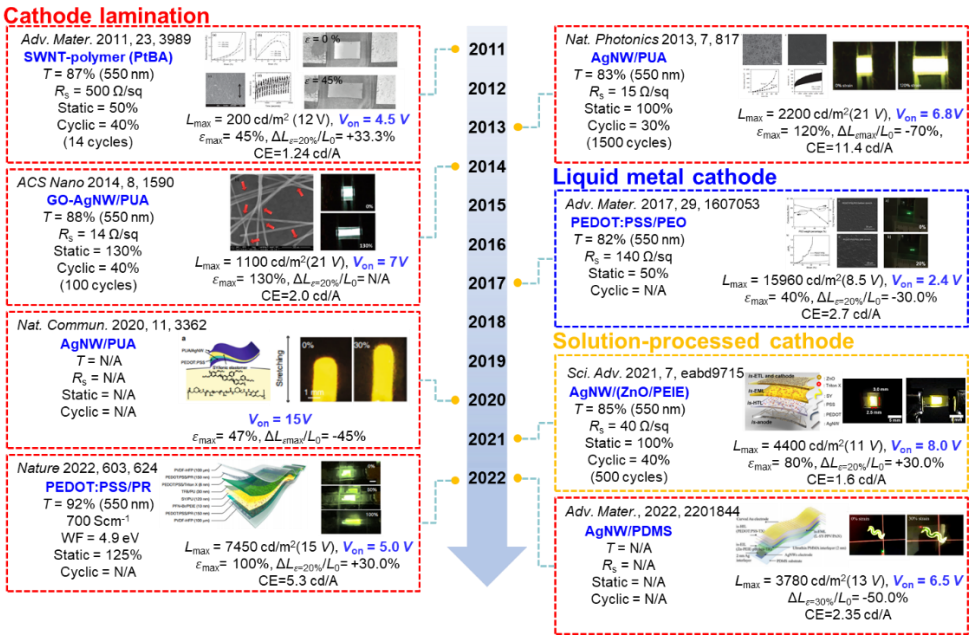

Figure 1.5 Roadmap of the development of stretchable electrodes and intrinsically stretchable light-emitting devices.

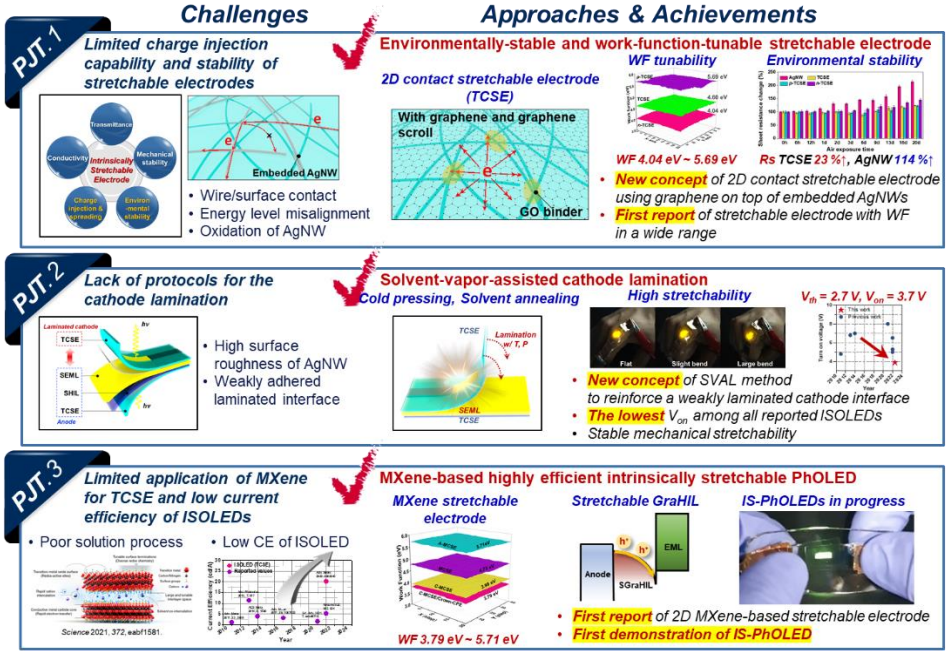

Figure 1.6 Challenges and achievements in this dissertation.

Chapter 2. Environmentally Stable and Work Function Tunable Graphene-based 2D-Contact Stretchable Electrodes for Intrinsically Stretchable Organic Light-Emitting Diodes

2.1. Introduction

Wearable electronics need a unified device that can be stretched to form intimate contact with human skin.[14,31-34] Such systems can use on-skin sensors to monitor physiological signals continuously in real-time, and can directly visualize signals by seamless incorporation of stretchable displays.[35-39] However, despite the significant improvement in stretchability of the devices, the development of intrinsically-stretchable displays was stagnated because of high operating voltages that are not suitable for human skins. The state-of-art stretchable displays that consist of fully-stretchable layers can be easily stretched > 100%, but are normally operated under an AC electric field of several kilovolts by using a high-voltage amplifier.[5,15-17]

As an alternative, DC-driven intrinsically-stretchable organic light-emitting diodes (ISOLEDs) are preferred, because they can be operated at much lower voltages, so they are more promising candidates for wearable applications.[18-23] Nonetheless, only several papers on DC-driven fully intrinsically stretchable LEDs using intrinsically stretchable emitting layers and electrodes have been reported since 2011 because of a technical issue that the strategies to improve the stretchability always degrades the device performance. The low performance of ISOLEDs can be attributed to the lack of stretchable electrode materials that can address poor charge injection at the widely used one-dimensional (1D) metal nanowire/organic layer interface. Therefore, it is very difficult to improve the

properties of stretchable electrodes.

Embedded silver nanowires (AgNWs) have been known as the most commonly used stretchable electrodes.[40,41] However, due to the limited contact area at the interface between the 1D AgNW and the organic layer, the embedded AgNWs show poor charge injection properties. The misaligned energy level at the stretchable electrode/organic layer interface of ISOLEDs is another issue that needs to be solved. In particular, it is difficult to achieve efficient electron injection in ISOLEDs without reactive alkali fluorides or metals as interlayers.[42] Recently, a stretchable electrode with a low work function (*WF*) exhibits only ~ 4.6 eV of *WF*, which is difficulty in efficiently injecting electron or hole charges at the cathode and anode, respectively.[34] Therefore it is necessary to align the energy levels at the each interface of two stretchable electrodes for increasing the performance of ISOLEDs.

Herein, a two-dimensional-contact stretchable electrode (TCSE) is designed using AgNWs as the conductive filler and graphene as the *WF* modifier on the surface, forming a two-dimensional electrical contact with the adjacent organic layer upon lamination. The *WF* of TCSE can be tuned up to 5.69 eV by *p*-type charge transfer doping, and down to 4.04 eV by *n*-type charge transfer doping. The *n*-TCSE is carefully laminated onto the active layer to form a complete two-dimensional electrical contact. TCSE contains graphene and graphene scroll layers on top of AgNW networks embedded in a styrene-ethylene-butadiene-styrene (SEBS) elastomer matrix. The graphene layer not only modifies the WF but also promotes charge diffusion and hinders the internal diffusion of oxygen and moisture, greatly improving charge injection and environmental stability. The mechanical stability of TCSE is improved due to the graphene scroll connecting cracks and graphene oxide (GO) bonding the NW-NW junction. With all these benefits, the ISOLED shows L_{max}

= 1130 cd/m^2, V_{on} = 5.5 V, CE = 9.3 cd/A, and a stable luminescence in continuous operation at 100 cd/m^2 with LT_{50} = 7.07h (the lifetime at 50% initial luminance under continuous operation).

2.2. Materials and Experiments

Single-layer graphene was grown on copper (Cu) foil by chemical vapor deposition. The Cu foil inserted into the quartz tube was heated to 1060 °C with 15 sccm of H_2 and then annealed for 30 min. In the graphene growth stage, the precursor CH_4 gas was flowed at 60 sccm for 30 min. The foil was then rapidly cooled to room temperature. The result was a graphene film with a uniform monolayer on Cu foil. A solution of poly(methyl methacrylate) (PMMA) (996k, Sigma-Aldrich) (4.6 g in 100 ml of chlorobenzene) was spin coated onto graphene/copper foil as a supporting polymer layer and then dried in air for 1 h. The Cu foil was then removed using an ammonium persulfate ($(NH_4)_2S_2O_8$) etchant for 5 h, then the PMMA/graphene film was floated in deionized water to rinse the residual etchant. Graphene, the back side of Cu without PMMA protection, is rolled into scrolls due to surface tension (33). After that, the graphene scrolls-decorated PMMA/graphene film was transferred to the target substrate and rinsed with acetone for 1 h to remove the PMMA support layer and leave the graphene WF modifier layer on the glass.

For the preparation of patterned *p*- and *n*-TCSEs, a pristine AgNW solution (30 nm × 30 μm, Novarial, 5 mg/mL in isopropyl alcohol) was diluted to 2.5 mg/mL and spin-coated twice on graphene at 2000 rpm for 60 s. Then, the electrode was heated at 125 °C for 10 min to increase the interaction at the AgNW/AgNW and AgNW/graphene interface. GO solution (2 mg/mL, H_2O dispersion, Sigma-Aldrich)

was diluted to 0.5 mg/mL with DIW and isopropyl alcohol and sonicated for 30 min to increase the dispersion of GO. Then, the electrode was immersed in the GO solution for 30 s, washed with deionized water, and then dried in air to perform a welding process. This step ensures the deposition of discontinuous GO in the AgNW junction.

Before the electrodes were surface-embedded in the SEBS matrix, the prepared electrodes were protected with a PDMS mask and then treated with oxygen plasma generated using reactive ion etching (RIE) to oxidize the AgNWs and remove the graphene. Exposed areas can be easily washed away with DIW.

For TCSE fabrication, a SEBS solution (180 mg/mL in toluene) was drop-cast onto the patterned electrodes and stored in ambient air until the solvent was completely evaporated. The thickness of the measured TCSE was 200 μm. The electrodes were then stripped from the substrate in water with AgNW/graphene fully embedded in the SEBS surface. TCSE was p-doped using a diluted solution of perfluorinated ionomer (PFI, 2 wt% in IPA) spin coated at 2000 rpm for 60 s. TCSE was n-doped using a spin-coated solution of polyethyleneimine (PEI, Sigma, 3 wt% in 2-methoxyethanol) at 3000 rpm for 60 s and annealed at 90 °C for 5 min.

To prepare the SHIL solution as the first step of fabrication of a unit cell and a passive matrix ISOLEDs, 5 wt% of Triton X-100 was added to poly(3,4-ethylenedioxythiophene):poly(styrenesulfonate) (PEDOT:PSS, Clevios™ P VP AI4083), and then the solution was diluted with isopropyl alcohol in a 1:1 weight ratio. Then 1.6 mg/mL of Triton X-100 was first dissolved in a solvent (toluene:cyclohexanone in a volume ratio of 1:4). And Super Yellow (PDY-132, Sigma, 8 mg/mL) was dissolved in the solution prepared in the previous step to obtain a SEML solution. The SHIL solution was first spin-coated on p-TCSE at 2000

rpm for 60 s and annealed at 90 °C in air for 10 min, leaving a film with a thickness of 150 nm. Continuous coating of SEML was performed in a glove box filled with N_2 at 3000 rpm for 60 s, and then the assembly was heat treated at 90 °C for 5 min. The final thickness of SEML was ~200 nm. The treated specimens were pre-contacted with n-TCSE under gentle pressure in a glove box.

For the lamination process, the specimens were hot pressed at a pressure of ~ 50 kPa for 5 min in air. Electrical contact was performed using Cu tape prior to encapsulation using 3M VHB tape. The linear stretching test for ISOLED was performed at a stretching rate of 0.5 mm/s.

The R_s of the TCSE was measured using a four-point probe coupled with a Keithley 2400 source meter. The light transmittance of TCSE was measured using ultraviolet (UV) absorption spectroscopy (Lambda 465, PerkinElmer). Raman spectroscopy was performed using LabRAM HR Evolution (HORIBA) with a 532 nm laser to confirm that the graphene layer was successfully transferred into the SEBS matrix. Surface topography images of the composite electrodes were obtained with an atomic force microscope (NX-10, Park Systems). The surface potential was analyzed using a Kelvin probe (KP Technology Ltd.). For the static stretching tests, strain up to 100% was applied using a homemade setup operated at a stretching rate of 10 mm/min. The cyclic stretching tests were repeated 0 to 40% strain for 500 cycles at a speed of 100 mm/min. In both tests, the change in electrical conductivity was measured in real time using a digital multimeter. Cross-sectional samples were prepared using a 30 kV gallium liquid metal ion source and a focused ion beam (FIB, SMI3050E) system and analyzed using a TEM (JEM-2100F). The *J-V-L* characteristics of the ISOLED were measured using a spectroradiometer with a source meter (CS2000, Konia Minolta).

2.3. Results and Discussion

The TCSE was composed of a graphene *WF* modifier exposed to air, conductive silver nanowire (AgNW) percolation networks beneath the graphene, graphene oxide (GO) binder at AgNW junctions to improve the stretchability, and molecular dopants to tailor the *WF* of TCSE on graphene **(Figure 2.1)**. The *WF* of the TCSE can be easily tuned by incorporation of the graphene *WF* modifier because of the unique property of the Dirac point arising from the crossing-point of π and π^* band of graphene.[43] The *p*-type doping of graphene using a perfluorinated ionomer (Nafion®) (*p*-dopant) that has highly-electronegative fluorine groups causes decrease in the electron density in graphene by spontaneous charge transfer from graphene to fluorine groups in Nafion; this decrease shifts the Fermi level E_F towards the valence band. On the contrary, polyethyleneimine (PEI, *n*-dopant) with unpaired electrons in nitrogen atoms increases the electron density, and thus shifts E_F to above the Dirac point **(Figure 2.1)**. To our best knowledge, this is the first demonstration of a TCSE that has *WF* in a wide range between 4.04 and 5.69 eV **(Table 2.1)**. Furthermore, the TCSE can form a two-dimensional uniform electric contact with the adjacent organic layer, and this contact spreads the charges to the two-dimensional graphene and significantly facilitates charge injection from the electrode to the adjacent layers.

AgNWs on graphene were surface-embedded into styrene-ethylene-butylene-styrene (SEBS) polymer matrix with graphene exposed to air. SEBS is a triblock copolymer with Young's modulus $10.3 \leq Y \leq 35$ MPa and can be stretched to > 500% of strain due to the existence of soft polybutylene and polyethylene blocks.[5] The estimation of the Hansen solubility parameter **(Table 2.2)** indicates that the

polyvinylpyrrolidone (PVP), the polymer ligand that wraps the AgNW during the synthesis, has higher miscibility with SEBS than widely-used polydimethylsiloxane (PDMS) does. Taken together, all these advantages prove the feasibility of the TCSE as a stretchable electrode for the ISOLEDs.

AgNW percolation networks commonly suffer from high junction resistance and weak wire-to-wire interaction that cause non-uniform electrical conductivity and poor stretchability.[21] Therefore, before embedding the AgNW and graphene in the SEBS elastomer, junctions of AgNWs were welded using graphene oxide (GO). Despite the insulating nature of GO [44], the sheet resistance R_s of the AgNW/graphene electrode can be significantly reduced from 38 Ω/sq to 24 Ω/sq by dipping the electrode in the GO solution for 0.5 min **(Figure 2.2)**. With increase in GO dipping time, R_s increased to 31 Ω/sq, whereas the transmittance T remained at ~ 89% with little change.

The variation in R_s after GO solution welding can be explained using the atomic force microscopy (AFM) topography of the AgNW/graphene surface **(Figure 2.3; Figure 2.4A to C)**. Given the radius ~ 30 nm of AgNWs, the capillary effect drives GO solution to fill the gaps of the AgNWs after 0.5 min of the treatment.[45] This junction-welding effect could significantly strengthen the interactions at the AgNW/AgNW interface and AgNW/graphene interfaces. With further increase in treatment time to 1.0 min, continuous and rigid GO thin film that had $Y = 32$ GPa [46] formed on the AgNW network surface and degraded the mechanical stability of the electrode. Hence, 0.5 min of GO solution welding was chosen as the standard condition for junction welding.

Then GO treated AgNW/graphene electrode surface was covered with SEBS solution (180 mg/mL in toluene) to form a 200-μm-thick SEBS layer on top. The

AgNW and graphene were peeled off the glass substrate and transferred to the SEBS surface with the graphene exposed to air and the AgNWs directly underneath it. This free-standing surface-embedded electrode was named TCSE.

In the TCSE with 0.5 min of GO solution welding, AgNW/AgNW and AgNW/graphene interfaces were maintained after embedding process; the TCSE had low R_s = 24 Ω/sq and high T = 89% **(Figure 2.5)**, which is almost comparable with that of AgNW/graphene electrodes on glass **(Figure 2.2)**. This result indicates a complete transfer of AgNW/graphene onto the SEBS surface without residuals on glass releasing substrate.

The presence of graphene on top of TCSE was first confirmed by cross-section transmission electron microscopy (TEM) **(Figure 2.6)**. Compared with the backside of the AgNW network as a reference, the high contrast on the surface of AgNW was proven to be graphene. Successful transfer of graphene to the substrate was also confirmed using Raman spectroscopy **(Figure 2.7)**. Two characteristic peaks of graphene at 1587 cm^{-1} (G band) and 2684 cm^{-1} (2D band) were observed in the TCSE [47], confirming that the transfer of graphene to SEBS elastomer matrix was successful and did not induce additional defects.

WF tunability of the TCSE was presented using Kelvin Probe *WF* mapping for a large area **(Figure 2.8)**. Compared with pristine TCSE, *p*-doped TCSE (*p*- TCSE) prepared using Nafion shows a high *WF* = 5.69 eV, whereas *n*- TCSE fabricated using a PEI showed a low *WF* = 4.04 eV, which is sufficient for injection of holes and electrons from electrodes to the adjacent organic layers. This is the first demonstration of TCSE for stretchable optoelectronics.

The charge carrier transporting properties of graphene of TCSE as a charge-spreading promoter were confirmed by Hall effect measurement. The carrier

mobility in graphene layer was superior to pristine AgNW networks **(Figure 2.9)**. Moreover, the surface carrier concentration of TCSE was nearly twice than that of pristine AgNW networks. This phenomenon was owing to the spontaneous redistribution of charges from AgNW to graphene showing high carrier mobility. This advancement means that the graphene sheet assists in spreading the charge carrier across TCSE.

The mechanical stability of TCSE was then evaluated using a static tensile test **(Figure 2.10)**. As expected, the TCSE with one layer of graphene with graphene scrolls (TCSE1) is more mechanically stretchable than pristine AgNW embedded in SEBS. The best stretchability was achieved using a triple layer of graphene with graphene scroll (TCSE3, R_s = 23.2 Ω/sq and T = 84%); the combination only had a normalized resistance change (R/R_0) of 1.8 at strain = 40%. The same trend was also observed in the cyclic stretching test at strain = 40% for 500 cycles **(Figure 2.11)**. The crumpling and interplay among multiple graphene layers can significantly reduce the Young's modulus, and hence increase the stretchability.[48,49]

Graphene is known to readily crack at strain < 5% because it has a strong carbon-carbon network that lacks a means of energy dissipation. Counterintuitively, intercalation of graphene scrolls could bridge the cracks to decrease the graphene layer's Young's modulus Y and increase the stretchability.[49] The graphene with graphene scrolls was first transferred onto the glass substrate and then embedded into the elastomer matrix after releasing process. Under strain = 40%, open cracks formed in the graphene layer, but graphene scrolls bridged them to maintain conduction paths **(Figure 2.12)**. AgNW percolation networks beneath the graphene can also bridge the cracks to maintain the electrical conductivity under stretching, so TCSE is more stretchable than pristine AgNW networks.

Then, the environmental stability of the pristine AgNW, TCSE, *p*-TCSE, and *n*-TCSE were evaluated by monitoring relative changes in R_s and *WF* at room temperature and relative humidity of 40% **(Figure 2.13)**. During exposure to these conditions for 20 d, the AgNW electrode was easily oxidized so its R_s increased by > 114%, and its *WF* increased by 15%. Oxidation of AgNW yields Ag_2O [50], which is non-conductive. However, incorporation of graphene on top of AgNW significantly improved the stability of TCSE. A layer of sp^2-hybridized carbon atoms in a hexagonal lattice can significantly block direct pathways of oxygen and water penetration, and this blockage decreases the oxidation of the AgNWs. After 20 days of exposure to air, *p*-doping with PFSA exhibited negligible changes in the *WF* and R_s of the *p*-TCSE, because PFSA has remarkable chemical stability.[51] Similarly, *n*-doping with PEI also exhibited better storage stability than that of pristine AgNW electrodes **(Figure 2.13)**. Hence, the environmental stabilities of *p*- and *n*-TCSE are sufficient to meet the processing standard for the electrode for the ISOLEDs.

A surface-modified TCSE was prepared for the lamination process of ISOLED's fabrication. To avoid using the direct coating of solution-processed cathode that might degrade the device operation lifetime, cathode lamination was adopted, because the electrode can be prepared on another substrate and then stacked on the organic layer without using a solvent. A miniature portable hot-press machine was used to apply temperature and stress to the sample for successful lamination.

Conductive poly(3,4-ethylenedioxythiophene) polystyrene sulfonate (PEDOT:PSS), a commercialized conducting polymer, serves as a hole injection layer in the light-emitting diodes. The stretchability of the pristine PEDOT:PSS shows a low fracture strain of 5% [52], so inclusion of non-ionic surfactant Triton X

facilitates self-assembly of PEDOT and PSS chains, and yields growth in the PEDOT and PSS domain sizes, to yield a stretchable HIL (SHIL) **(Figure 2.14)**.

Before ISOLED fabrication, the AgNW/graphene on the glass was patterned using a photoresist-free reactive ion etching (RIE) method, then embedded in the SEBS elastomer matrix. The *WF* modifier graphene can also serve as a sacrificial layer that is easily etched by the oxygen plasma and washed away after the patterning process **(Figure 2.15)**. The electrode then was embedded in SEBS and used as the cathode for ISOLEDs.

Current density–voltage–luminance (*J-V-L*) relationships show maximum luminance L_{max} = 1130 cd/m^2 and turn-on voltage V_{on} = 5.5 V. And the maximum CE of ISOLED was achieved at L = 228 cd/m^2 with CE = 9.3 cd/A **(Figure 2.16)**. Then the ISOLED was tested in a constant-current mode until failure in a glove box with initial luminance of 100 cd/m^2, showing LT_{50} = 7.07 h **(Figure 2.17)**.

The stretching-tolerance of the ISOLED unit cell was measured by sandwiching it between 3M VHB tapes as encapsulation. The initial luminance of the ISOLED unit cell decreased to 71.8% after application of 20% strain, and kept decreasing with further stretching **(Figure 2.18A, B)**. This study demonstrates the superiority of TCSEs over previous stretchable electrodes for ISOLED applications **(Table 2.3)**.

2.4. Conclusion

In this research, ISOLEDs with stable charge injection at the electrode interface have been developed by designing a TCSE that consists of AgNW percolation network as the conductive filler, two-dimensional graphene as the *WF* modifier exposed to air, GO binder to increase conductivity and stretchability, and dopants to control the *WF*. The *WF* of the TCSE can be tailored from 4.04 to 5.69 eV to fulfill

the required energy-level alignment with reduced the charge-injection barrier. Besides, the formation of a two-dimensional continuous electrical contact at the TCSE/organic interface is vital for efficient charge injection, and the ISOLED shows L_{max} = 1130 cd/m^2, V_{on} = 5.5 V, CE = 9.3 cd/A, and a stable light-emission with LT_{50} = 7.07h. Using these tactics, a three-inch five-by-five passive matrix ISOLED also proves the feasibility of the doped TCSE as the electrode and the lamination for large-scale applications.

However, the device stability needs to be further improved for practical applications of ISOLEDs. In order to increase the stability, stretchable encapsulation materials should also be developed. There are several requirements to realize the stable encapsulation materials. Their *Y* must be matched with those of substrates and active layers to avoid delamination at the encapsulation and ISOLED interface. Furthermore, they must adhere strongly to the substrate to avoid sliding of the device that can result in an irreversible deformation of the ISOLED. Finally, to protect from oxidation, the encapsulants must have low water and oxygen vapor transmission rate. The stretchability and the barrier property of encapsulation are always contradictory because the former requires densely-packed polymer whereas the second requires a highly-entangled polymer chain. Hence, innovations are required in the designing of encapsulation materials to increase the chemical and mechanical stability of ISOLEDs.

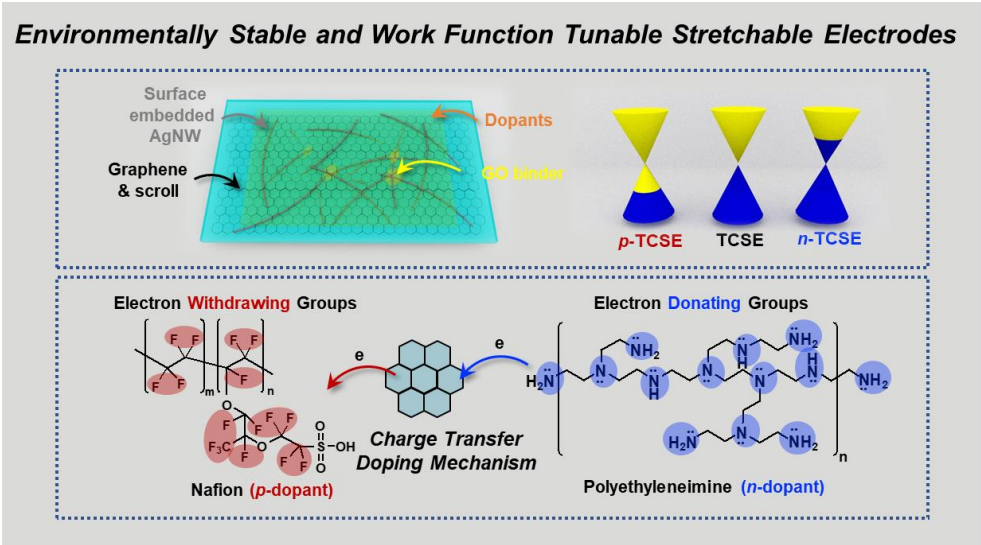

Figure 2.1. Conceptual illustration of environmentally stable and work function tunable graphene-based 2D-contact stretchable electrode (TCSE) and its p- and n-type charge transfer doping mechanism using Nafion and polyethyleneimine, respectively.

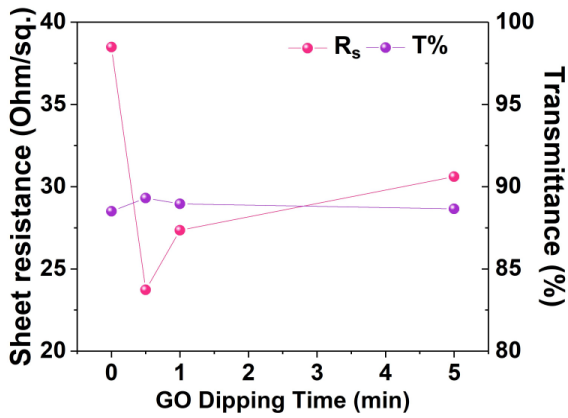

Figure 2.2. The change in sheet resistance and transmittance of AgNW/graphene electrodes in terms of GO dipping time.

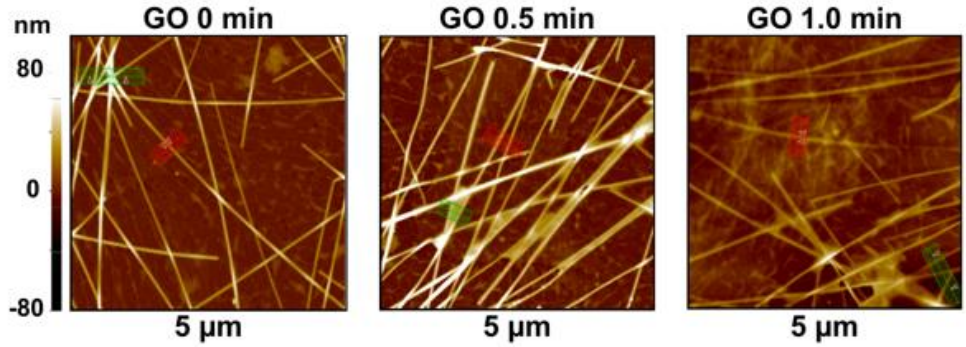

Figure 2.3. Atomic force microscopy (AFM) topography of the AgNW /graphene electrodes fabricated on a rigid glass substrate with GO solution treatment for 0, 0.5, or 1.0 min.

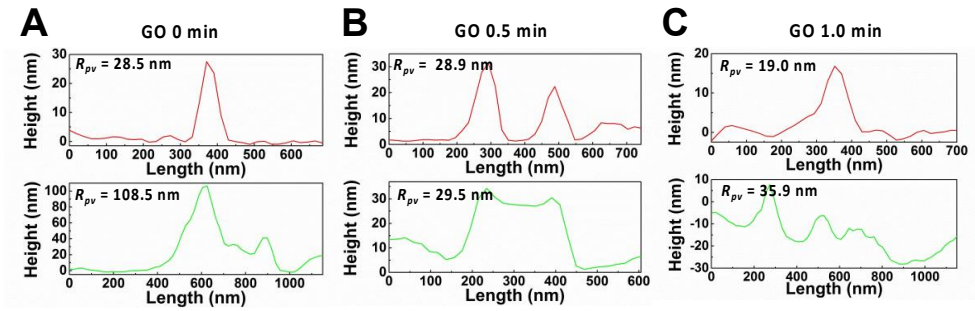

Figure 2.4. (A to C) AFM line profiles of the AgNW/graphene electrode on a glass substrate with 0, 0.5, and 1 min of GO solution dipping. Red and green lines represent the AFM line profiles at different spots as indicated in Figure 2.3.

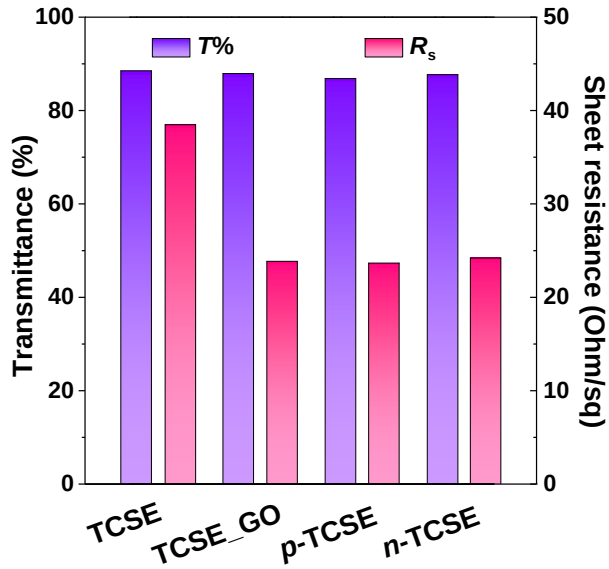

Figure 2.5. Transmittance T and sheet resistance R_s of pristine TCSE, TCSE with graphene oxide (GO) dipping, and TCSE after *p*- and *n*-type doping.

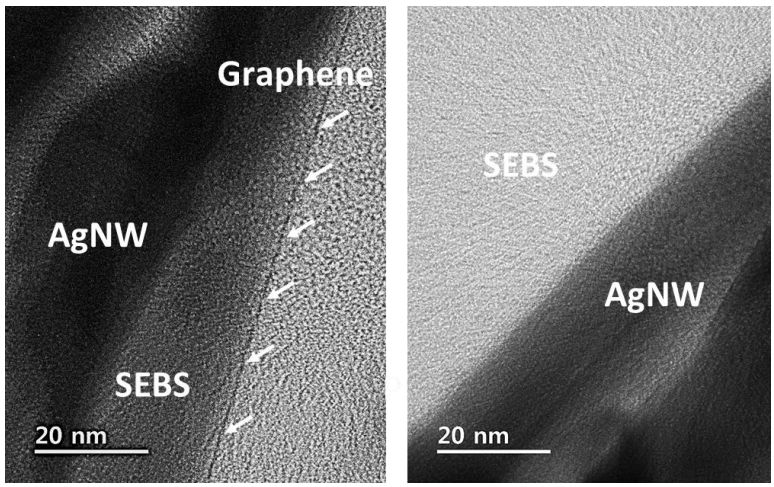

Figure 2.6. Transmission electron microscopy (TEM) cross-section images of TCSE.

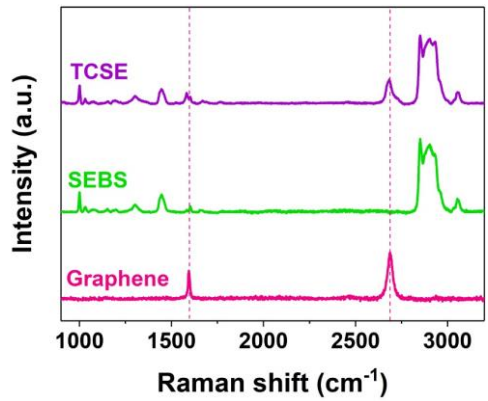

Figure 2.7. Raman spectroscopy of pristine graphene, SEBS, and TCSE.

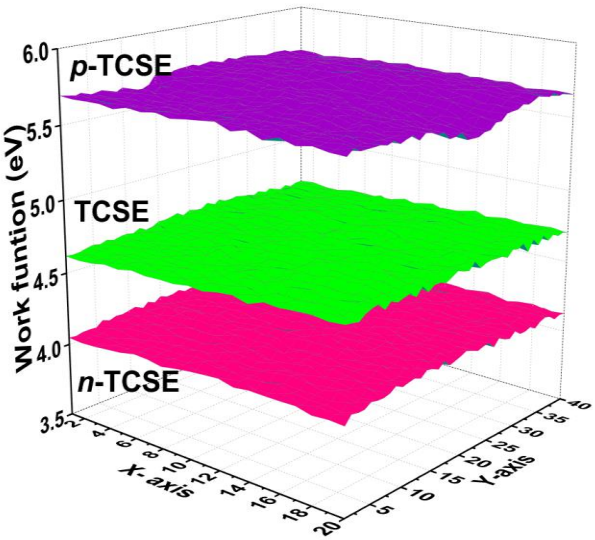

Figure 2.8. Kelvin probe mapping of *WF* of TCSE before and after *p*- and *n*-type doping. Each step in the x- and the y-axis represents 635 nm.

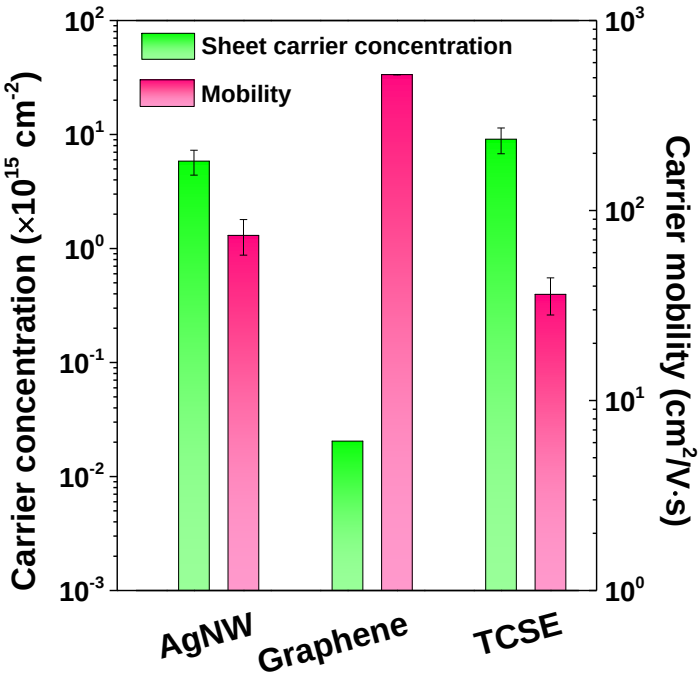

Figure 2.9. Sheet carrier concentration and carrier mobility of AgNW, graphene, and TCSE evaluated using Hall effect measurement.

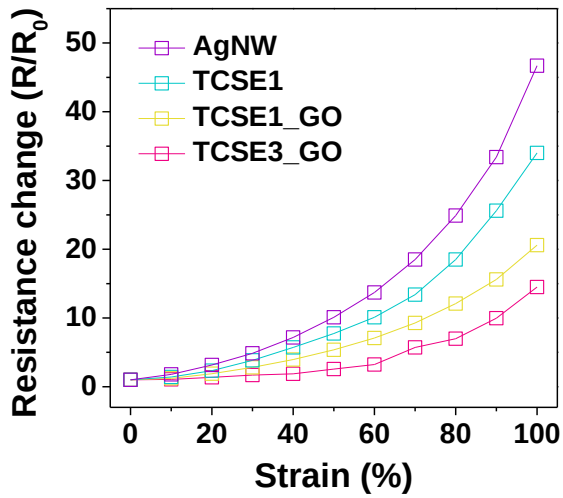

Figure 2.10. Static stretching test of AgNW, TCSE, and TCSE with multiple layers of graphene before and after graphene oxide (GO) treatment.

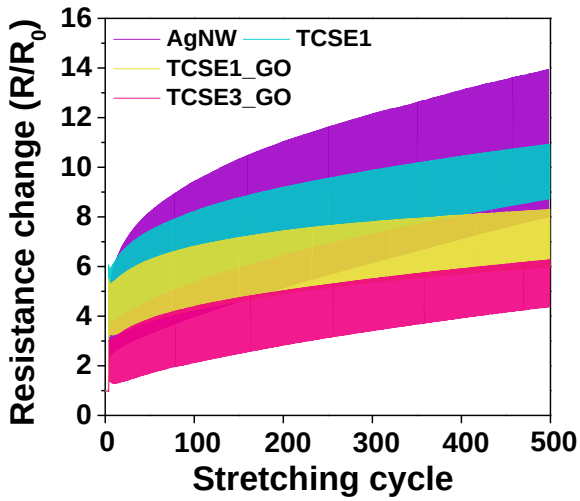

Figure 2.11. Cyclic stretching tests (strain = 40%) of AgNW, TCSE, and TCSE with multiple layers of graphene before and after graphene oxide (GO) treatment.

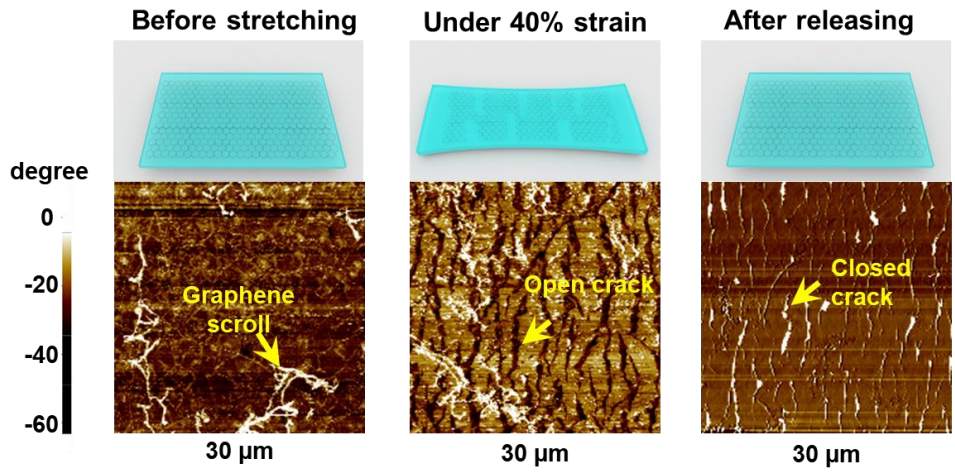

Figure 2.12. Atomic force microscopy (AFM) phase images taken during the in-situ stretching test (strain = 40%) on graphene that had been transferred onto SEBS.

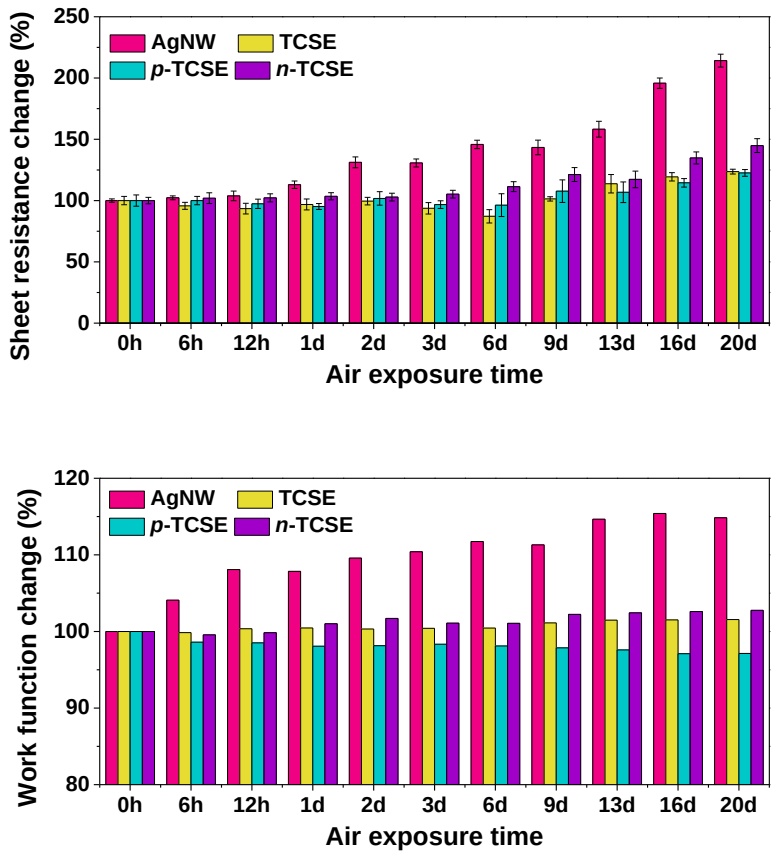

Figure 2.13. Environmental stability test on AgNW, TCSE, and *p*- and *n*-TCSE in terms of R_s and *WF* change at room temperature and relative humidity of 40%.

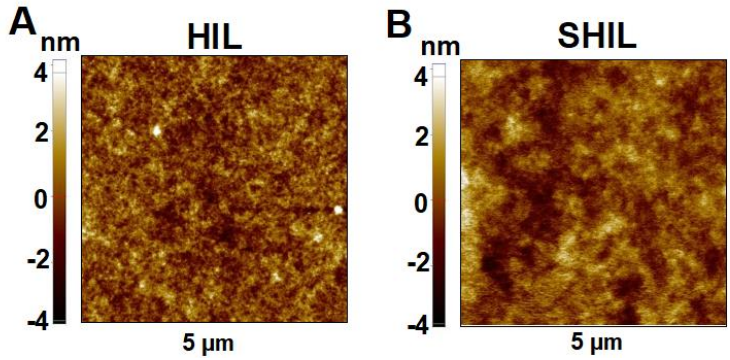

Figure 2.14. AFM topography of (A) pristine hole injection layer (HIL) using PEDOT:PSS, (B) stretchable HIL (SHIL) with the addition 10 wt% of non-ionic surfactant Triton X-100 into PEDOT:PSS.

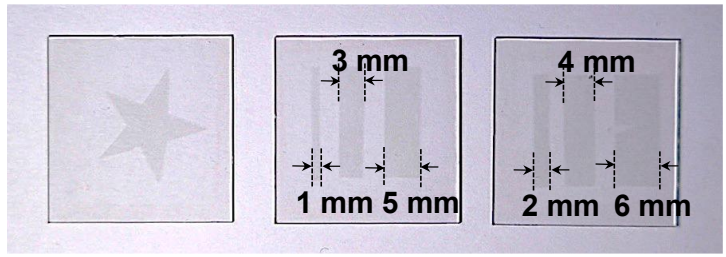

Figure 2.15. Optical microscopic image of photo patternable TCSE using reactive ion etching.

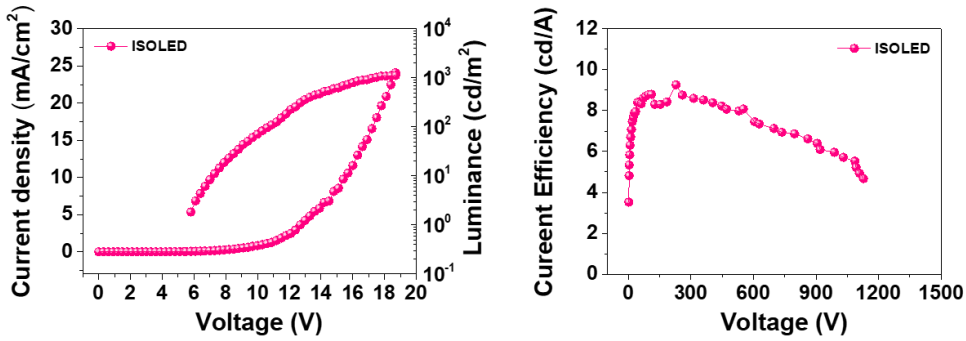

Figure 2.16. Current density-voltage-luminance (*J-V-L*) and current efficiency-luminance characteristics of ISOLED.

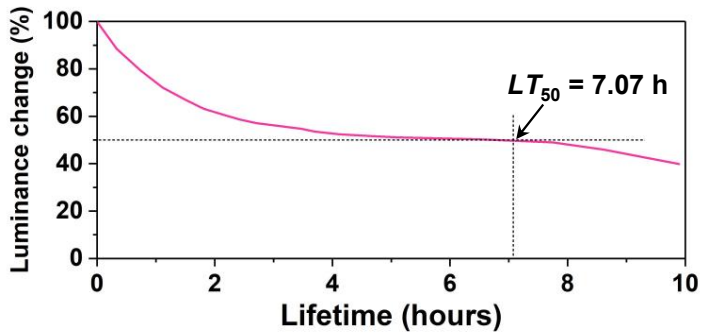

Figure 2.17. The accelerated lifetime of ISOLED with initial luminance at 100 cd/m^2 in N_2-filled glove box.

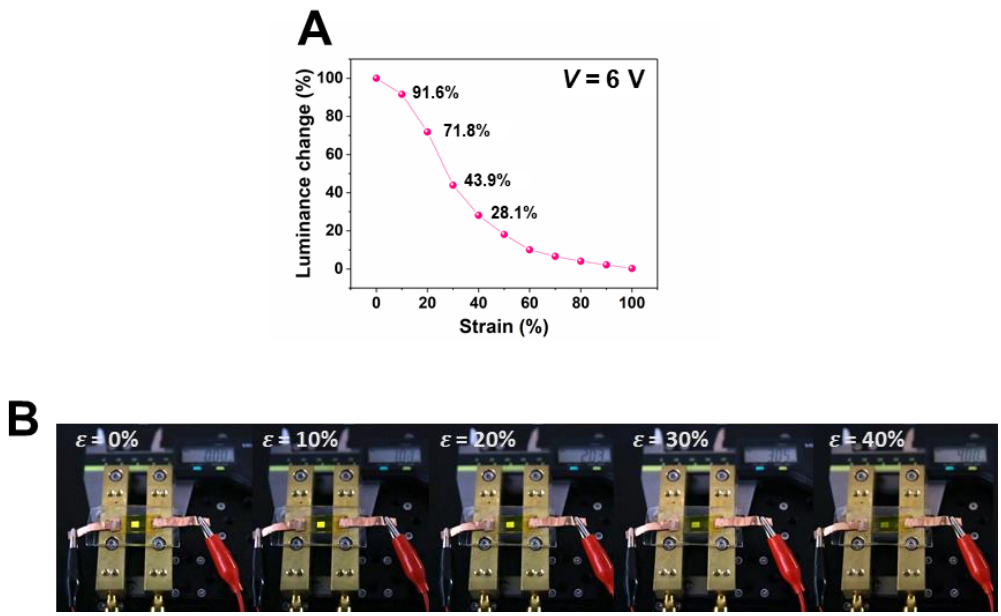

Figure 2.18. (A) Change in luminance of ISOLED at 6 V *vs* tensile strain. (B) Photographs of ISOLED unit cell under tensile stretching.

Table 2.1. Comparison of electrodes for intrinsically stretchable didoes

Electrodes	*R*s (Ω/sq)	*T* (%)	R/R_0 (ε = 40 %)	Cyclic stretching (cycles)	Cyclic stretching (R/R_0)	Roughness (nm)	*WF* (eV)	Ref.
TCSE	24	88	3.9	500, ε = 40 %	6.1	6.5 (R_a)	5.69 (*p*-type) 4.04 (*n*-type)	this work
PH1000:AI4083:FS30 PH1000: FS30	-	-	-	-	-	-	5.35 4.73	(1)
ZnO/PEIE/AgNWs/PEIE/ZnO	40	85	5	500, ε = 40 %	11	-	-	(2)
AgNWs-GO/PUA	14	82.5	3.2	100, ε = 40 %	3	10 (R_{pv})	-	(3)
AgNWs/PUA	15	83	10	1500, ε = 30 %	4.3	3.4 (R_{pv})	-	(4)
SWNT/PtBA	500	87	1.45	14, ε = 40 %	1.14	10 (R_a)	-	(5)
AgNWs/Aerogel/PDMS	15	80	4	100, ε = 25 %	0.8	17 (R_{pv})	-	(6)
AgNWs/CF/PDMS	15	85	15	200, ε = 35 %	3.7	23 (R_{rms})	-	(7)
AgNWs/Ethanolamine/Chitosan	8.4	89	11	100, ε = 30 %	1.38	-	-	(8)

(1) N. Matsuhisa, S. Niu, S. J. K. O'Neill, J. Kang, Y. Ochiai, T. Katsumata, H.-C. Wu, M. Ashizawa, G.-J. N. Wang, D. Zhong, X. Wang, X. Gong, R. Ning, H. Gong, I. You, Y. Zheng, Z. Zhang, J. B. H. Tok, X. Chen, Z. Bao, High-frequency and intrinsically stretchable polymer diodes. *Nature* **600**, 246-252 (2021).

(2) J. H. Kim, J. W. Park, Intrinsically stretchable organic light-emitting diodes. *Sci. Adv.* **7**, eabd9715 (2021).

(3) J. Liang, L. Li, K. Tong, Z. Ren, W. Hu, X. Niu, Y. Chen, Q. Pei, Silver Nanowire Percolation Network Soldered with Graphene Oxide at Room Temperature and Its Application for Fully Stretchable Polymer Light-Emitting Diodes. *ACS Nano* **8**, 1590-1600 (2014).

(4) J. Liang, L. Li, X. Niu, Z. Yu, Q. Pei, Elastomeric polymer light-emitting devices and displays. *Nat. Photonics* **7**, 817-824 (2013).

(5) Y. Zhibin, N. Xiaofan, L. Zhitian, P. Qibing, Intrinsically Stretchable Polymer Light-Emitting Devices Using Carbon Nanotube-Polymer Composite Electrodes. *Adv. Mater.* **23**, 3989-3994 (2011).

(6) J. Kim, J. Park, U. Jeong, J. W. Park, Silver nanowire network embedded in polydimethylsiloxane as stretchable, transparent, and conductive substrates. *J. Appl. Polym. Sci.* **133**, 43830 (2016).

(7) Y. Chen, R. S. Carmichael, T. B. Carmichael, Patterned, Flexible, and Stretchable Silver Nanowire/Polymer Composite Films as Transparent Conductive Electrodes. *ACS Appl. Mater. Interfaces* **11**, 31210 (2019).

(8) S. B. Park, J. W. Han, J. H. Kim, A. F. Wibowo, A. Prameswati, J. Park, J. Lee, M. W. Moon, M. S. Kim, Y. H. Kim, Multifunctional Stretchable Organic–Inorganic Hybrid Electronics with Transparent Conductive Silver Nanowire/Biopolymer Hybrid Films. *Adv. Opt. Mater.* **9**, 2002041 (2021).

Table 2.2. Hansen solubility parameters of materials and calculated distance in the Hansen space

Hansen solubility parameter	δ_D [MPa]	δ_P [MPa]	δ_H [MPa]	R
PVP	15.5	11.6	8.6	-
Polydimethylsiloxane	15.9	0.1	4.7	6.1
Polyurethane	18.1	9.3	4.5	3.5
Polystyrene	21.3	5.8	4.3	6.8
Polybutylene	16.9	2.5	4	5.3
Polyethylene	17.1	3.1	5.2	4.8

Table 2.3. Performance of stretchable electrodes for ISOLEDs

Year	Electrodes	*R*s (Ω/sq)	*T* (%)	R/R_0 (ε = 40 %)	Cyclic stretching (cycles)	Roughness (nm)	*WF* (eV)	Ref.
2011	SWNT/PtBA	500	87	1.45	14 @ ε = 40 %	10 (R_a)	-	(1)
2013	AgNWs/PUA	15	83	10	1500 @ ε = 30 %	3.4 (R_{pv})	-	(2)
2014	AgNWs-GO/PUA	14	82.5	3.2	100 @ ε = 40 %	10 (R_{pv})	-	(3)
2016	AgNWs/Aerogel/ PDMS	15	80	4	100 @ ε = 25 %	17 (R_{pv})	-	(4)
2019	AgNWs/CF/PDMS	15	85	15	200 @ ε = 35 %	23 (R_{rms})	-	(5)
2021	AgNWs/Ethanolamine/Chitosan	8.4	89	11	100 @ ε = 30 %	-	-	(6)
2021	ZnO/PEIE/AgNWs/PEIE/ZnO	40	85	5	500 @ ε = 40 %	-	-	(7)
2021	PH1000:AI4083: FS30 PH1000: FS30	-	-	-	-	-	5.35 4.73	(8)
2022	PEDOT:PSS/PR	700 S cm^{-1}	92	1.8	-	-	4.9	(9)
This work	TCSE Environmental stability	24	89	3.9	500 @ ε = 40 %	6.5 (R_a)	5.69 4.04	-

(1) Y. Zhibin, N. Xiaofan, L. Zhitian, P. Qibing, *Adv. Mater.* 23, 3989-3994 (2011).
(2) J. Liang, L. Li, X. Niu, Z. Yu, Q. Pei, *Nat. Photonics* 7, 817-824 (2013).
(3) J. Liang, L. Li, K. Tong, Z. Ren, W. Hu, X. Niu, Y. Chen, Q. Pei, *ACS Nano* 8, 1590-1600 (2014).
(4) J. Kim, J. Park, U. Jeong, J. W. Park, *J. Appl. Polym. Sci.* 133, 43830 (2016).
(5) Y. Chen, R. S. Carmichael, T. B. Carmichael, *ACS Appl. Mater. Interfaces* 11, 31210 (2019).
(6) S. B. Park, J. W. Han, J. H. Kim, A. F. Wibowo, A. Prameswati, J. Park, J. Lee, M. W. Moon, M. S. Kim, Y. H. Kim, *Adv. Opt. Mater.* 9, 2002041 (2021).
(7) J. H. Kim, J. W. Park, *Sci. Adv.* 7, eabd9715 (2021).
(8) N. Matsuhisa, S. Niu, S. J. K. O'Neill, J. Kang, Y. Ochiai, T. Katsumata, H.-C. Wu, M. Ashizawa, G.-J. N. Wang, D. Zhong, X. Wang, X. Gong, R. Ning, H. Gong, I. You, Y. Zheng, Z. Zhang, J. B. H. Tok, X. Chen, Z. Bao, *Nature* 600, 246-252 (2021).
(9) Z. Zhang, W. Wang, Y. Jiang, Y.-X. Wang, Y. Wu, J.-C. Lai, S. Niu, C. Xu, C.-C. Shih, C. Wang, H. Yan, L. Galuska, N. Prine, H.-C. Wu, D. Zhong, G. Chen, N. Matsuhisa, Y. Zheng, Z. Yu, Y. Wang, R. Dauskardt, X. Gu, J. B. H. Tok, Z. Bao, *Nature* 603, 624-630 (2022).

Chapter 3. Holistic Protocol to Achieve Reliable Electrode Lamination in Intrinsically Stretchable Organic Light-Emitting Diodes with Low-Voltage Operation

3.1. Introduction

Wearable electronics systems integrated with on-skin sensors and stretchable displays can be used to monitor and visualize physiological signals continuously.[5,14,31,32,34,49,52-60] However, despite the significant improvement in stretchability of electronic devices, the development of intrinsically-stretchable displays has stagnated because they require high operating voltages that are not suitable for wearable applications.[36-39,61-63] The state-of-the-art stretchable displays that consist of fully-stretchable layers can be easily stretched > 100%, but are normally operated under an AC electric field of several kilovolts by using a high-voltage amplifier. As an alternative, DC-driven ISOLEDs are preferred, because they can be operated at low voltages, so they are more promising candidates for practical applications. Nonetheless, few papers have reported ISOLEDs that use intrinsically stretchable emitting layers and electrodes since 2011.[19,20,22,23,64-67] The reported DC-driven ISOLEDs still suffer from the high V_{on} > 5 V that strongly depends on the quality of the contact between the stretchable cathode and light-emitting materials.

Direct coating of conductive nanomaterial composites can be used to form an electrical contact at the interface, but this method requires a careful selection of the solvent for electrode deposition.[23] Alternatively, a free-standing stretchable cathode can be prepared on another substrate and then contacted onto the active layer with heat T and pressure P to enhance the adhesion strength.[66] This is referred to as the

lamination method for stacking the cathode material onto the active layer of ISOLED. However, the rough surface of the stretchable electrode at the laminated interface and its huge difference in surface energy from the underlying organic layer causes poor adhesion, which requires fine-tuning of the lamination conditions. No standards related to the cathode lamination process have been reported. Due to difficulties in quantifying the lamination quality, excess T, P, or both are often applied during lamination to improve stretchability, but these treatments induce a significant decrease in conductivity of electrodes and photoluminance (PL) intensity of the light-emitting layer.[66,68-70] Therefore, the excess T and P substantially increase the V_{on} and decrease the device efficiency. Simultaneous attainment of low V_{on} and excellent stretchability with a firmly laminated interface remains a difficult challenge; overcoming it requires development of new methods to eliminate those demerits.

Here, we present a solvent-vapor-assisted lamination (SVAL) method to reinforce the weakly laminated stretchable cathode interface. This method substantially increases the mechanical stretchability and lowers the operation voltage of the ISOLEDs. Achieving a uniform contact and strong adhesion at the interface is the key to attaining reliable lamination. A cold-pressing (CP) treatment was introduced to reduce the surface roughness R_{rms} of silver nanowires (AgNWs) before the embedding process, which enables the stretchable cathode to form a uniform contact at the laminated interface. After the subsequent SVAL treatment, an increase in adhesion of the laminated interface is attributed to the increase in segmental motion of polymer chains in the partially-solvated active layer. The cross-hatch pattern analysis is also proposed to better quantify the adhesion properties of the laminated interface. The CP treatment and subsequent SVAL substantially decrease the

threshold voltage V_{th} from 6.7 to 2.7 V. The ISOLED also exhibits excellent mechanical stretchability, with no significant change in luminance under 30% strain.

3.2. Materials and Experiments

Graphene synthesis and transfer process were described previously.[66] Pristine AgNW solution (30 nm in diameter, 30 μm in length, Novarial, 5 mg/mL dispersed in isopropyl alcohol) was diluted to 2.5 mg/mL to increase the uniformity of the AgNW electrode. The diluted AgNW solution was spin-coated on top of graphene at 2000 rpm for 60 s twice, then the combination was heated at 150 ℃ for 5 min to evaporate the residual solvent and weld the junctions between AgNWs. To reduce sheet resistance R_s of the TCSE, a portable hot-press machine was used for the CP process. The surface of AgNW/graphene was covered with another glass substrate, which was then pressed at 50 kPa for 2 min to flatten the surface of AgNW percolation networks and reduce R_s. Then styrene-ethylene-butadiene-styrene (SEBS, 180 mg/mL in toluene) was drop-cast on the as-prepared AgNW/graphene substrate and left in ambient air to allow the solvent to evaporate. Then the substrate was released from the glass substrate in water with AgNW and graphene fully embedded in SEBS.

To prepare a stretchable hole-injection layer (SHIL), 5 wt% of Triton X-100 was added to a 1:1 weight ratio solution of poly(3,4-ethylenedioxythiophene):poly(styrenesulfonate) (PEDOT:PSS, Clevios™ P VP AI4083) in isopropyl alcohol. The stretchable light-emitting layer (SEML) solution was a blend of Super Yellow (Merck, PDY-132, 10 mg/mL in cyclohexanone), polyethylene oxide (PEO, MW = 5m, 10 mg/mL in cyclohexanone), and potassium

trifluoromethanesulfonate (KCF_3SO_3, 10 mg/mL in cyclohexanone) at a volume ratio of 10:6:1. Perfluorinated sulfonic acid (PFSA, 2 wt% in IPA) and polyethyleneimine (PEI, Sigma, 3 wt% in 2-methoxyethanol) solutions were prepared as the *p*- and *n*-type dopant respectively for the TCSEs.

The TCSE with PFSA coating was used as the anode, and the TCSE with PEI coating was used as the cathode. The SHIL was spin-coated onto the TCSE anode at 1000 rpm for 60 s and then annealed at 90 ℃ for 5 min in ambient air. A successive coating of SEML at 3000 rpm for 60 s was performed under N_2 atmosphere in a glove box with both O_2 and H_2O < 1 ppm. The resultant thickness of SEML was ~ 200 nm. Then the substrate was kept in a closed petri dish on a hot plate at 100 ℃ with an open plastic Petri dish (60 × 15 mm) filled with desired organic solvents for 5 min. The organic solvent partially solvates the surface of the SEML, and thereby increases the adhesion at the interface. The treated specimen was taken out swiftly, then pre-contacted with the active layer by application of gentle pressure in the glove box. The specimen was hot pressed at 50 kPa and 100 ℃ for 5 min in ambient air by using the hot-press machine, then encapsulated using 3M VHB tape. The reference structure fabricated on ITO substrate was the same with that of ISOLED except for the cathode. After coating of SEML, LiF (1nm) and Al (100 nm) were sequentially deposited using a thermal evaporator.

The surface topographic images of TCSEs before and after CP were obtained by atomic force microscopy (NX-10, Park Systems). Surface morphologies of TCSE before and after CP were compared using scanning electron microscopy (SEM). Optical microscopy was also used to characterize the change in AgNW before and after thermal annealing. The R_{rms} of materials for the ISOLED were characterized using atomic force microscopy (NX-10, Park Systems). A cross-section sample of

ISOLED was prepared using a focused ion beam (FIB, SMI3050E), then analyzed using TEM (JEM-2100F) with a beam energy of 30 kV. For static stretching test, tensile strain was applied to the electrode using a homemade stretcher with at 20 mm/min. The cyclic stretching test on the electrode was conducted from 0 to 40% for 500 cycles at 100 mm/min. The change in resistance was measured using a digital multimeter (Keithley 6500) in real time.

The *J-V-L* characteristics of ISOLED were measured using a spectroradiometer (CS2000, Konia Minolta) combined with a source meter. For the stretching test, the strain was applied using a homemade stretcher with a Maya 2000 spectrometer placed right on the top of the ISOLED. The whole stretching system was placed in a dark box to exclude the effect of light from the environment.

To evaluate the adhesion at the interface between SEML and TCSE, a cross-hatch pattern was created using stacked razor blades with a 1-mm separation. The pattern was created to exclude the effect of cohesion forces within the film. After the SVAL process, the TCSE was peeled off slowly.

3.3. Results and Discussion

AgNW percolation networks are normally embedded in the elastomer surface to attain stretchability. Nonetheless, the charge transport in the stretchable electrode was only allowed along the wire and the contact area between half-buried AgNW networks and the adjacent organic material is limited.[66] Hence, charge transport and injection in AgNW-based stretchable electrodes were inefficient. To boost the efficiency of the ISOLED, we developed two-dimensional contact stretchable electrode (TCSE) as both anode and cathode in our previous work.[66] Graphene was

introduced on the surface of embedded AgNW networks to form a two-dimensional contact with the organic material. Carrier mobility, work function tunability, and contact area of the TCSE have been significantly improved because of the graphene interlayer.[66]

To fabricate an ISOLED, the TCSE was formed on another substrate, and adhered to the stretchable light-emitting layer (SEML) by using *T* and *P*; this process is known as cathode lamination (**Figure 3.1A**). Adhesion at the interface between TCSE and SEML requires both strong interactions across the interface, and a uniform contact area. Whereas, applying excess *T*, *P*, or both during lamination to increase interfacial adhesion can deteriorate the conductivity of the electrode and the light-emitting property of SEML and thereby degrade the device's electrical and physical characteristics. SVAL was, therefore, developed to reinforce a weakly-laminated interface to attain improved stretchability without inducing any degradation during lamination. Since light-emitting polymers are mostly dissolved in non-polar solvents, so toluene and cyclohexanone, which have different boiling points (bps) were chosen as solvents for the solvent vapor treatment (**Figure 3.1B**). The segmental motion of polymer chains from the partially-solvated SEML surface is increased, so the polymer chain entanglement and interfacial adhesion also increase.

Forming a uniform contact at the laminated interface is vital for attaining strong interfacial adhesion. The CP process has been adopted to reduce R_{rms} of randomly-distributed AgNW percolation networks and thereby improve lamination quality (**Figure 3.1C**). AgNWs commonly suffer from high contact resistance R_c, so post-fabrication thermal annealing on AgNWs was used to weld the AgNW/AgNW junctions and reduce R_s. Thermal annealing has a more dominant effect than CP

treatment on R_s, so the effects of thermal annealing and CP on R_s of AgNW/graphene electrodes were evaluated separately.

R_s of the AgNW/graphene electrode substantially reduced from 38.4 Ω/sq at 25 ℃ to 21.4 Ω/sq after thermal annealing at 150 ℃ for 5 min (**Figure 3.2A**); this change indicates a reduction in contact resistance at the welded AgNW junctions. With further increasing annealing temperature to 200 ℃, AgNWs melted and became disconnected in the OM image (**Figure 3.3**); this change led increased R_s by a few orders of magnitude. Welding of AgNWs before embedding into the elastomer can prevent AgNWs from disconnecting and sliding at the junction, and thereby increases stretchability.[64] Then the effect of CP was evaluated using pristine AgNW/graphene without thermal annealing as the reference. R_s of the AgNW/graphene electrode declined by 19.1% after 2 min of CP at 50 kPa (**Figure 3.2B**) but increased to 38.2 Ω/sq after CP for 3 min. The change in morphology of AgNW/graphene before and after CP indicates that AgNWs were deformed by pressure to increase the compactness of structure with the underlying graphene layer (**Figure 3.2C,D**). The R_{rms} of the AgNW/graphene electrode has been significantly decreased from 62.1 to 50.9 nm with the CP treatment. However, severe deformation of AgNWs after 3 min of CP could degrade the charge transport along a wire; this change causes an increase in R_s. For these reasons, we chose 2 min for the CP process. After embedding in styrene-ethylene-butadiene-styrene (SEBS) elastomer matrix, the R_{rms} of TCSE prepared after CP decreased from 11.7 to 8.1 nm in 10 × 10 μm scan size (**Figure 3.2E,F**). Hence, the optimal post-fabrication treatment on AgNW/graphene was identified as thermal annealing at 150 ℃ for 5 min, followed by 2 min of CP at 50 kPa, showing a slight decrease in R_s to 21.0 Ω/sq.

The mechanical stretchability of the TCSE with and without any treatments was

evaluated. The TCSE with thermal welding and CP treatments showed only a 132% increase at 20% of strain, while the resistance of the control electrode increased by 181% at the same condition (**Figure 3.2G**). The same trend was also observed in the cyclic stretching test at 40% strain as expected (**Figure 3.2H**). The combination of thermal welding and CP treatments substantially suppress the sliding of the AgNW and enhance stretchability of the TCSE.

Then the effects of temperature and duration of lamination were evaluated by measuring the contact resistance R_c of two TCSE that faced each other. Lamination temperature was decided considering the glass transition temperatures T_g of components in the SEML. The segmental motion of the polymer chain increases at $T > T_g$, and this motion increases interchain diffusion with a firmly laminated interface. Polyethylene oxide (PEO) and polyethyleneimine (PEI) which were used in this work both have $T_g < 0$ ℃, so the chain mobility was assumed to be high at room temperature. However the light-emitting polymer (Super Yellow) has the highest $T_g = 85$ ℃, the lamination temperature should be maintained > 85 ℃ to ensure high polymer chain segmental motion but without inducing degradation in both TCSEs. Conductive surfaces of TCSEs were placed facing each other, and R_c was measured while T was increased from 90 to 130 ℃. R_c was lowest after one-time lamination at 100 ℃; this result indicates that the TCSE forms a good electrical contact without any degradation at the interface (**Figure 3.4A, B**).

Except for a uniform and flat stretchable electrode surface, increasing the interchain diffusion of polymer chains is also important to obtain a firmly laminated interface. Maintaining lamination temperature > T_g increases the mobility of the polymer chain, whereas a firmly-laminated interface without inducing degradation in device V_{on} cannot easily be obtained. Hence, monitoring variation of the PL

spectrum may be an indirect way to quantify the lamination quality. Toluene (bp = 110.6 °C) and cyclohexanone (bp = 155.6 °C) were chosen as solvents because they are commonly used to dissolve Super Yellow. To perform the solvent-vapor treatment, solvents were pre-heated separately in closed Petri dishes at 100 °C for > 5 min, then TCSE coated with the SEML was heated to form a partially-solvated surface. The difference in bps of the solvents caused opposing trends in PL of the SEML during the solvent vapor treatment. The use of cyclohexanone yielded a constant increase in PL intensity (**Figure 3.5A**) whereas the use of toluene yielded a decrease (**Figure 3.5B**). The normalized PL spectra of the same processes (**Figure 3.6**) were also displayed.

The presence of solvent on the SEML protects it from contact with air, and thereby avoids exciton quenching induced by oxygen. Solvent annealing using cyclohexanone for 5 min was the optimal condition for the lamination.[71] However, due to the low bp of toluene, it readily evaporates when heated at 100 °C, and does not solvate the SEML surface. Cross-sections of laminated ISOLEDs were analyzed to confirm the quality of the interface after lamination. The specimen was prepared using a focused ion beam, then analyzed using high-resolution transmission electron microscopy (HR-TEM) (**Figure 3.5C**). The TEM images showed no voids at the interface; this absence indicates that the TCSE formed intimate contact with the SEML layer.

To quantify the interfacial adhesion strength using adhesion test, we developed a cross-hatch pattern-transfer method (**Figure 3.5D**). The pattern created on the SMEL was intended to exclude the effect of the cohesion force of the SEML during the adhesion test (**Figure 3.7**). The area of the transferred SEML (*t*-SEML, dark area) was measured using image analysis after the monochrome adjustment to obtain a

high image contrast. The strength of the adhesion was quantified using the transfer rate *TR*, which was defined as the ratio of the area of transferred SEML (*t*-SEML) to the total area of SEML. A high *TR* means a strong adhesion at the laminated interface. The SVAL treatment using cyclohexanone for 5 min gave the highest *TR* = 0.839 (**Figure 3.5E**), while the SVAL treatment using toluene for 5 min gave significantly lower *TR* = 0.543 (**Figure 3.8**). The difference in *TR* indicates that the laminated interface after SVAL using toluene was weak, and this inference is consistent with the PL contour plots of solvent annealing using different solvents (**Figure 3.5A,B**). Therefore, the adhesion test reveals that the SVAL using cyclohexanone gives the best adhesion strength at the laminated interface, which is beneficial for the ISOLED operation.

When the voltage is applied to the ISOLED, ions in the SEML dissociate and drift to the opposite electrode to form electric double layers (EDL) that can induce severe band bending at electrode interfaces **(Figure 3.9A)**. This response facilitates charge injection without the need for a sophisticated device structure. Current density–voltage (*J*-*V*) relationships, especially at low operation voltage before turn-on, imply that the interface formed after CP and SVAL treatments is highly uniform with low leakage current when compared with the control group without any additional treatment (**Figure 3.9B**). In the *J*-*V* curve with both CP and SVAL treatments, two sudden increases in *J*, one between 0 and 1 V and one at > 2.7 V, are consequences of charge injection of holes and electrons, respectively. In Super Yellow, holes are more mobile than electrons[72], so the rate of charge injection is limited by electron transport. Hence, the second abrupt increase in *J* corresponds to the electron injection to the SEML layer. But the V_{th} of the control ISOLED, and the one with only CP are as high as 6.7 and 6.0 V, respectively, which implies that both CP and SVAL

treatments can significantly reduce the V_{th} with a better electron injection capability. The luminance-voltage (*L*-*V*) also exhibited the same trends as the *J*-*V* characteristics. The emitted light was detected using the spectroradiometer at V_{on} = 3.7 V with the maximum luminance L_{max} = 1754 cd/m^2 after SVAL (**Figure 3.9C**). To our best knowledge, this is the lowest V_{on} among all reported ISOLEDs (**Figure 3.9D, Table 3.1**).

The charge injection property of the ISOLED was compared with the ITO-based device that has the same device architecture except for the cathode. The ITO-based device had a lower V_{th} of 2.0 V than that of the ISOLED (**Figure 3.10, Table 3.1**); the difference is mainly induced by the difference in the electron injection barriers. The LiF/Al is the well-known cathode material that can significantly reduce the height of the electron injection barrier[73], whereas the AgNW/graphene (called TCSE in this work) with only PEI as the interlayer showed a work function of 4.04 eV[66], which makes electron injection in the ISOLED a rate-determining step for light-emission. Also, the voltage at which current efficiency is maximum was lower in the ITO device than in the ISOLED, proving that the LiF/Al electrode has better electron injection property than the TCSE. Therefore, the low V_{th} of the ISOLED (2.7 V) is slightly higher than that of the ITO device (2.0 V). Comparison of the *J*-*V*-*L* characteristics of the ISOLED with those of ITO, demonstrates that the suggested SVAL treatment yields cathodes that function well.

Before the ISOLED stretching test, microstructures of the stretchable organic layers were analyzed. The inclusion of non-ionic surfactant Triton-X into poly(3,4-ethylenedioxythiophene):polystyrenesulfonate (PEDOT:PSS) facilitates the self-assembly of PEDOT and PSS chains to yield a stretchable hole injection layer (SHIL, **Figure 3.11A,B**). The SEML that is deposited on the SHIL is incorporated with

polyethylene glycol (PEO) and salts to form a stretchable solid-state electrolyte. The stretchability of SEML originates from an interpenetrating polymer network in which Super Yellow forms a continuous network and the soft ionic conductive phase PEO fills the pores, in a way that mimics a sponge immersed in water.[74] As a result of the huge difference in polarities of Super Yellow and PEO, strong phase separation was induced between the Super Yellow and the soft ionic phase that contains PEO and KCF_3SO_3 (**Figure 3.11C,D**). Benefit from the microstructural engineering on SHIL and SEML, an *in-situ* tensile stretching test of the SHIL/SEML/PEI film on a homemade stretcher measured a crack-onset strain of ~ 70% **(Figure 3.12)**.

The ISOLED were sandwiched between 3M VHB tape to protect them from exposure to air before the stretching test. The initial luminance (100%) of the ISOLED showed a slight decrease only to 94% by 6% after the application of 20% strain, and the light emission spectrum did not change (**Figure 3.9E**). With a further increase of strain to 30%, the ISOLED that had been treated with CP and SVAL showed negligible degradation (**Figure 3.9F**). However, the control ISOLED and the one with only CP degraded rapidly as strain was increased to 20%. This difference in stretchability is attributed to the interface reinforced by the SVAL.

To perform a cyclic stretchability test in air, we evaluated the operation stability of the ISOLED first in air under constant voltage. 3M VHB tape is a poor barrier to oxygen and moisture, so the *L* of ISOLED at 8 V showed a monotonic decline after reaching the maximum luminance L_{max} and degraded to 50% within 2 min (**Figure 3.13A**), making the effect of cyclic mechanical strain cannot be easily distinguished from degradation caused by air. The *L* of ISOLED with both CP and SVAL treatments decreased after tens of cycles of stretching at 20% of strain (**Figure**

3.13B), despite its excellent static stretchability (**Figure 3.9E**). To demonstrate the stretchability of the ISOLED, it has been placed onto the joint of hand and can withstand large deformation when the hand makes a fist (**Figure 3.9G**).

Appropriate encapsulation can effectively delocalize the strain around minor defects and suppress crack formation in the film.[75] Hence, stretchable encapsulation design is critical to the cyclic stretchability of the device. Stretchability requires the encapsulant to be as amorphous as possible, but this requirement conflicts with the need for highly-crystalline polymer structure to provide a good barrier to oxygen and water. These two properties are always in conflict, and to meet both simultaneously requires innovations in encapsulation material design.

3.4. Conclusion

We present an SVAL method to reinforce a weakly laminated cathode interface, thereby substantially increasing the mechanical stretchability, and lowering the V_{on} of ISOLEDs. Achieving a uniform contact and strong adhesion at the interface is the key to attaining reliable lamination. The CP treatment has significantly reduced the R_{rms}, which enables the stretchable cathode to form a uniform contact at the laminated interface. After subsequent SVAL using cyclohexanone with a high boiling point, the surface of the SEML was partially solvated and the segmental motion of polymer chains was increased; these changes substantially reinforce the weakly laminated interfaces. The cross-hatch pattern analysis we propose here well quantified the adhesion properties of the laminated interfaces after SVAL. The CP and subsequent SVAL substantially decrease the V_{th} from 6.7 to 2.7 V. The ISOLED showed no significant change in luminance under 30% of strain; i.e., has excellent

mechanical stretchability. This work will provide a solution to the chronic adhesion problem that occurred at the laminated stretchable cathode interface of ISOLEDs, and will stimulate academic and industrial research on the fundamentals of stretchable optoelectronics for practical applications.

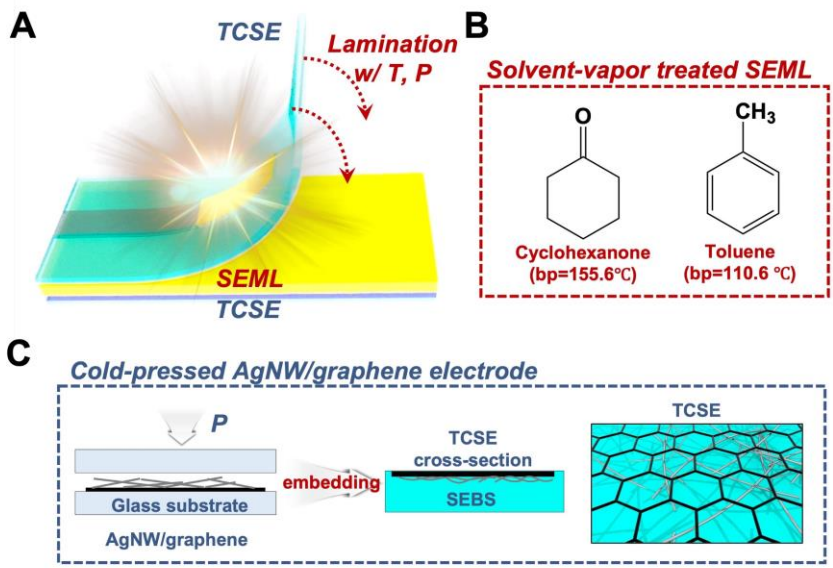

Figure 3.1. (A) Schematic illustration of cathode lamination process with the application of heat *T* and pressure *P* to obtain a firmly-laminated interface. Two-dimensional contact stretchable electrodes (TCSEs) as anode and cathode. (B) Chemical structures and boiling point (bp) of solvents used for vapor treatment before the lamination process. (C) Conceptual illustration of a cold-pressing method to reduce the surface roughness of AgNW/graphene electrode before surface embedding.

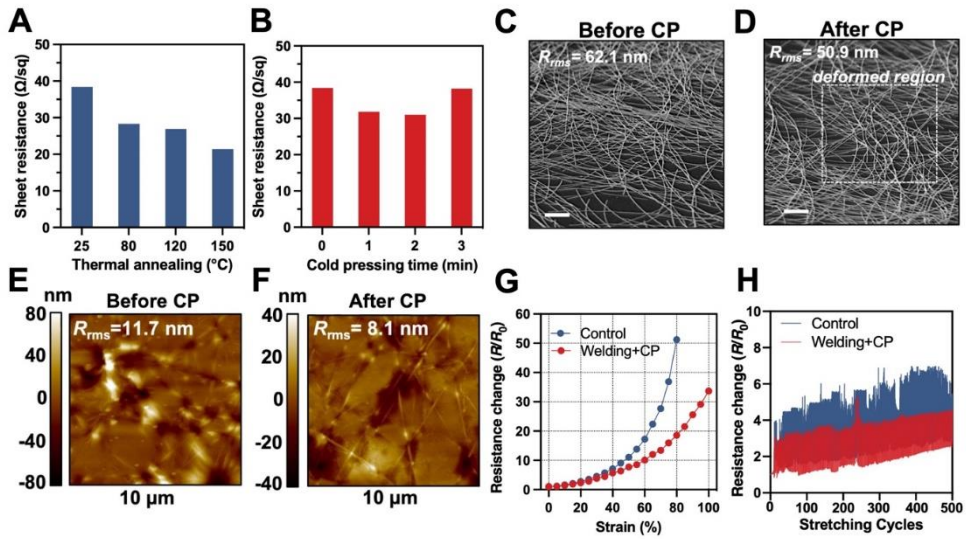

Figure 3.2. Evolution of sheet resistance of AgNW/graphene electrode on a glass substrate in terms of (A) thermal annealing at the desired temperature for 5 min, and (B) increasing CP time at 50 kPa pressure without thermal annealing. (C) and (D) SEM images of AgNW/graphene electrodes before and after CP. Scale bar: 1 μm. The dashed square region highlights the deformed AgNWs after CP. (E) and (F) AFM topography images (scan size: 10 × 10 μm) of AgNW/graphene electrode before and after CP. (G) Static stretching and (H) cyclic stretching tests (tensile strain = 40%) of the TCSE without any treatments (control) and the one with both thermal welding and CP treatments.

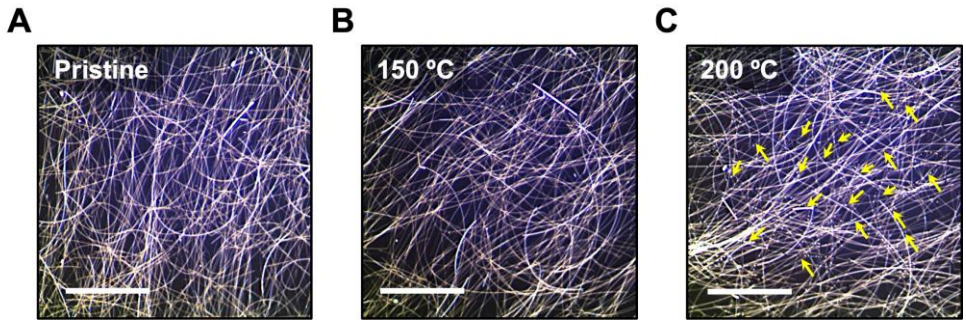

Figure 3.3. Optical microscopic images of AgNW/graphene electrode on the glass substrate (A) before annealing, and after annealing for 5 min at (B) 150 ℃ or (C) 200 ℃. Yellow arrows pointing towards white spots in AgNW networks indicate the disconnected AgNWs after high-temperature annealing at 200 ℃. Scale bar: 30 μm.

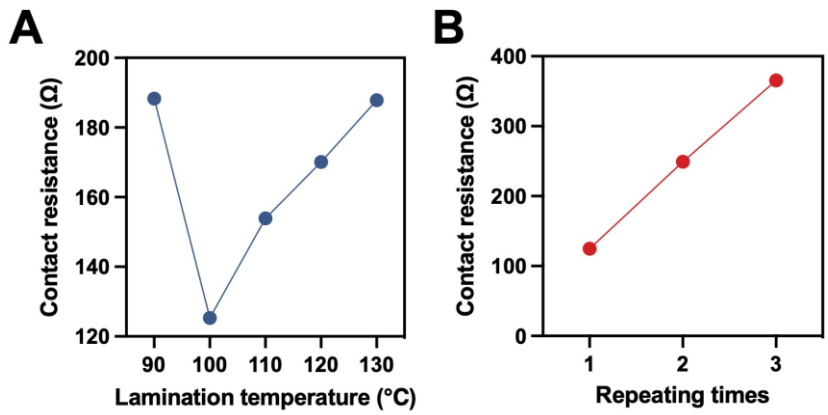

Figure 3.4. Evolution of contact resistance between two TCSEs with their conductive surface faced each other regarding varying (A) lamination temperature and (B) number of lamination processes.

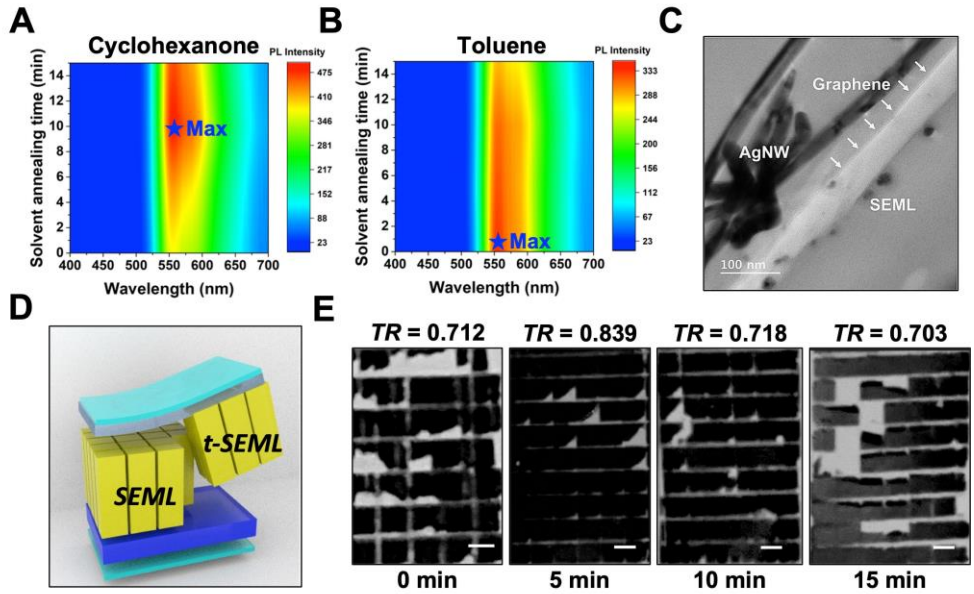

Figure 3.5. Photoluminance (PL) color plot after applying increasing duration of solvent vapor treatment using (A) cyclohexanone, and (B) toluene. (C) transmission electron microscopy cross-section images of the interfaces in the ISOLEDs. (D) Schematic illustration of the cross-hatch adhesion test. *t*-SEML stands for stretchable SEML transferred to the TCSE after the adhesion test. (E) Image analysis on the releasing substrate after detaching the cathode TCSE with increasing cyclohexanone solvent treatment time. Scale bar: 1 mm.

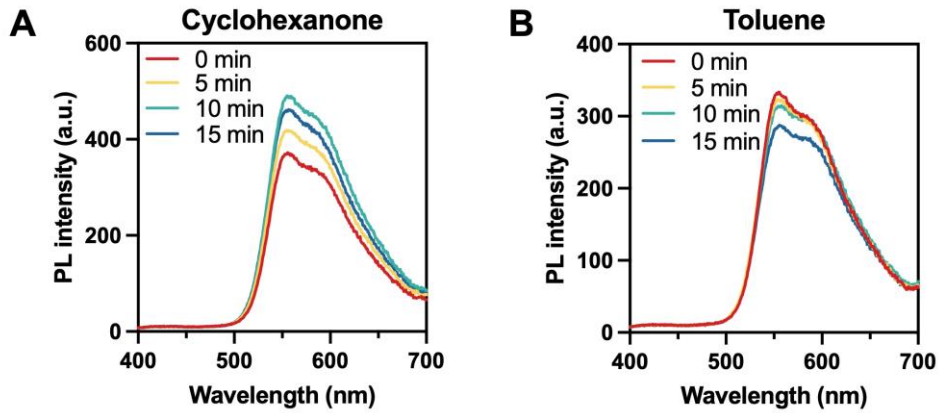

Figure 3.6. Evolution of steady-state PL spectra of the SEML with solvent vapor treatment at 100 ℃ using (A) cyclohexanone, or (B) toluene.

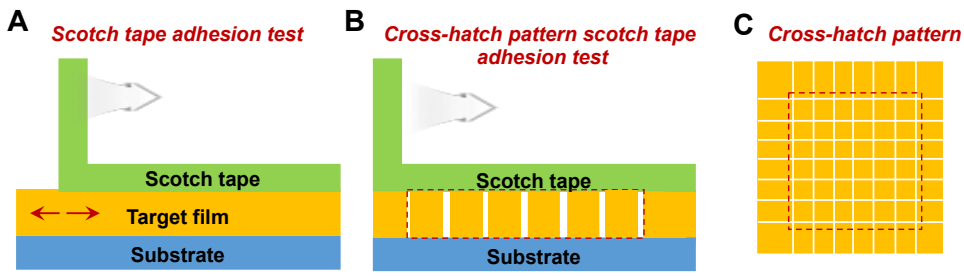

Figure 3.7. Side view of (A) conventional scotch-tape adhesion test and (B) cross-hatch pattern adhesion test. The red arrows in target film: directions of cohesion force in the SEML. (C) Top view of a typical cross-hatch pattern used in this study. Red dotted line: pattern analyzed for the adhesion evaluation

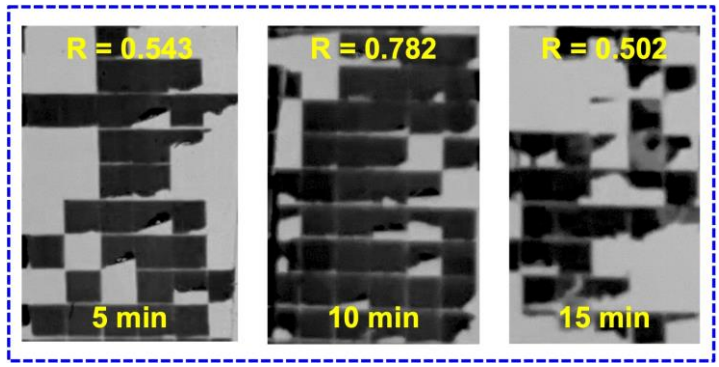

Figure 3.8. Image analysis after detaching the cathode TCSE with increasing toluene solvent treatment time. Scale bar: 1 mm.

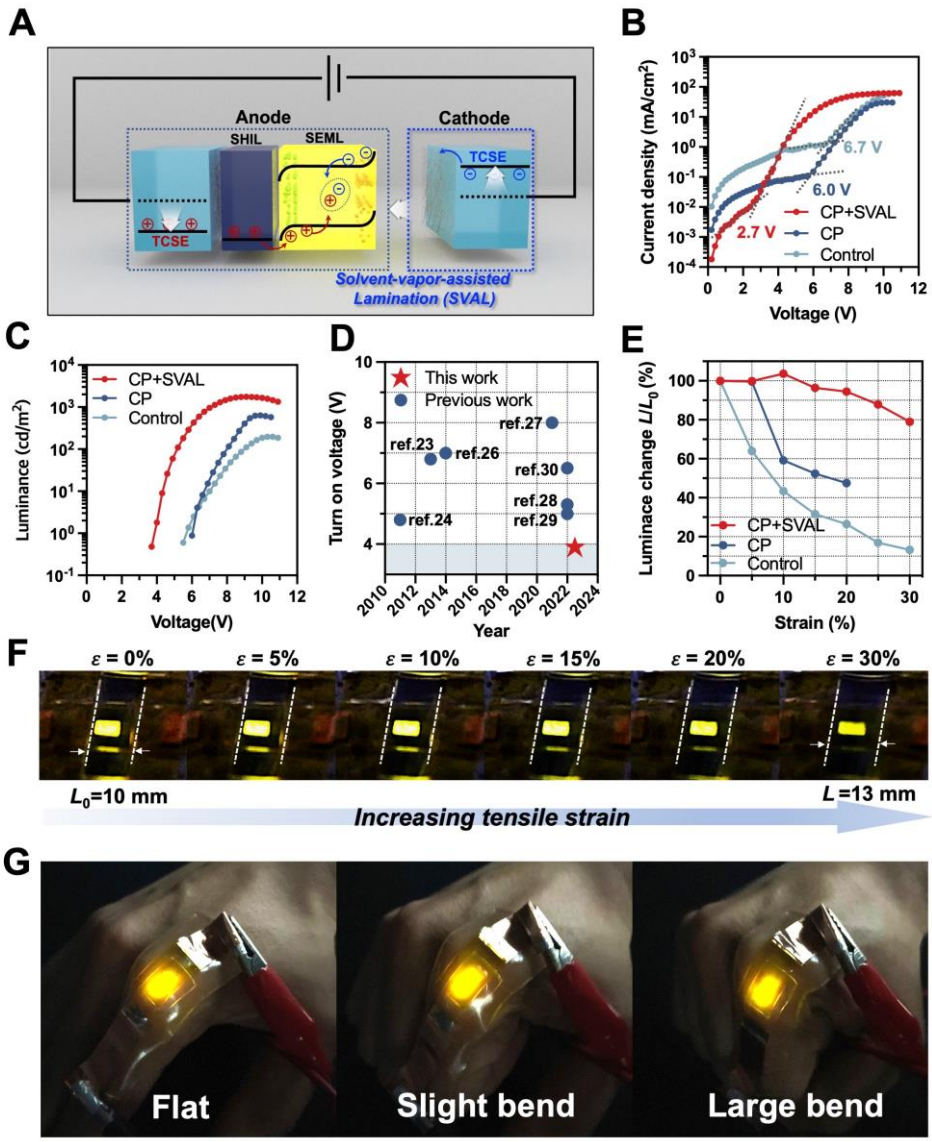

Figure 3.9. (A) Schematic image of ISOLED architecture fabricated using SVAL. SHIL: stretchable hole injection layer; SEML: stretchable light-emitting layer (see experimental section for more details). (B) Current density-voltage (*J-V*), and (C) luminance-voltage (*L-V*) of control ISOLED without any treatment, the ISOLED with CP and the ISOLED with both CP and SVAL. (D) Progress in the development of turn-on voltage V_{on} of ISOLEDs. (E) Change in luminance of the control ISOLED,

the one with only CP and the one with both CP and SVAL treatments at 6 V under uniaxial tensile strain. (F) Digital images of the ISOLED with both CP and SVAL treatments under tensile strain from 0 to 30% at 6 V. (G) Digital images of the ISOLED with both CP and SVAL treatments on the joint withstanding various deformations when making a fist.

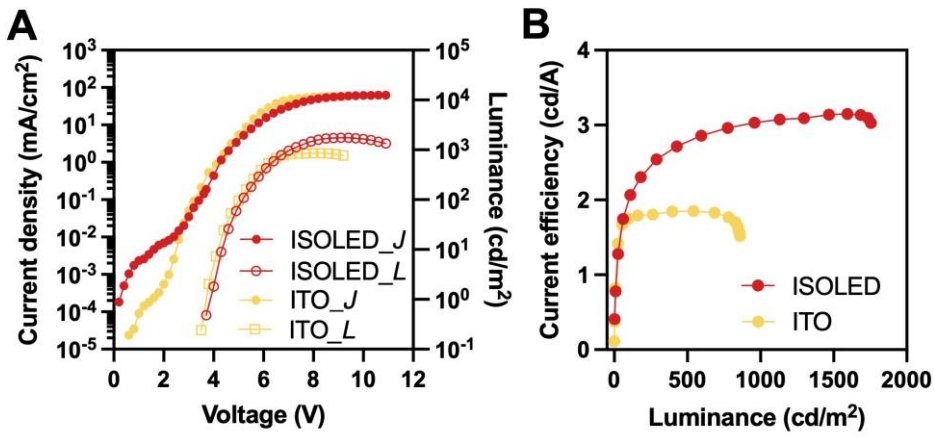

Figure 3.10. (A) Current density (*J*)-voltage (*V*)-luminance (*L*), (B) current efficiency characteristics of the organic light-emitting diode fabricated using the indium tin oxide (ITO) electrode on the glass substrate (0.7 mm) and the ISOLED with both CP and SVAL treatments. ITO device architecture: ITO (70 nm)/SHIL (150 nm)/SEML(~200 nm)/LiF (1 nm)/Al (~100 nm).

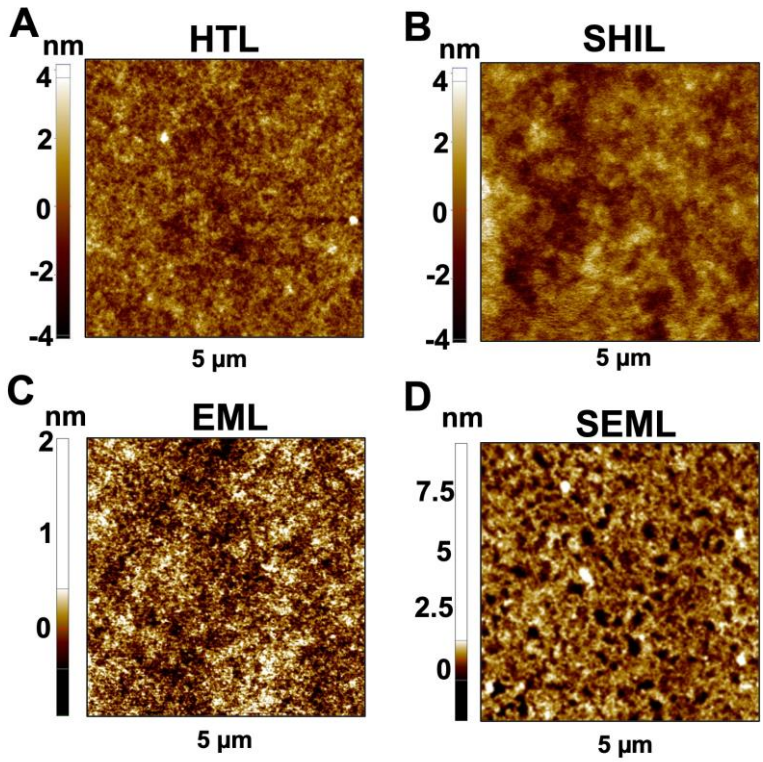

Figure 3.11. AFM topography (scan size: 5 × 5 µm) of (A) pristine hole injection layer (HIL) using PEDOT:PSS, (B) stretchable HIL (SHIL) with the addition of 5 wt% of non-ionic surfactant Triton X-100 into PEDOT:PSS, (C) pristine light-emitting layer (EML) Super Yellow, and (D) SEML that is composed of SY, PEO, and KCF_3SO_3.

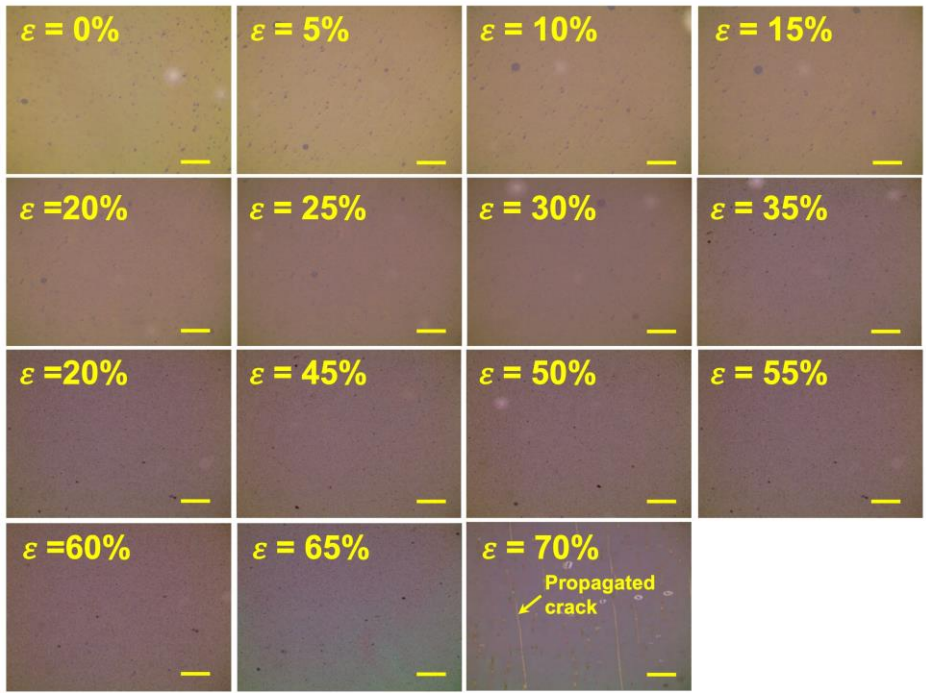

Figure 3.12. Optical microscopic images of *in-situ* stretching test on TCSE/SHIL/SEML/PEI/TCSE to demonstrate the stretchability of the organic layers. Scale bar: 150 μm.

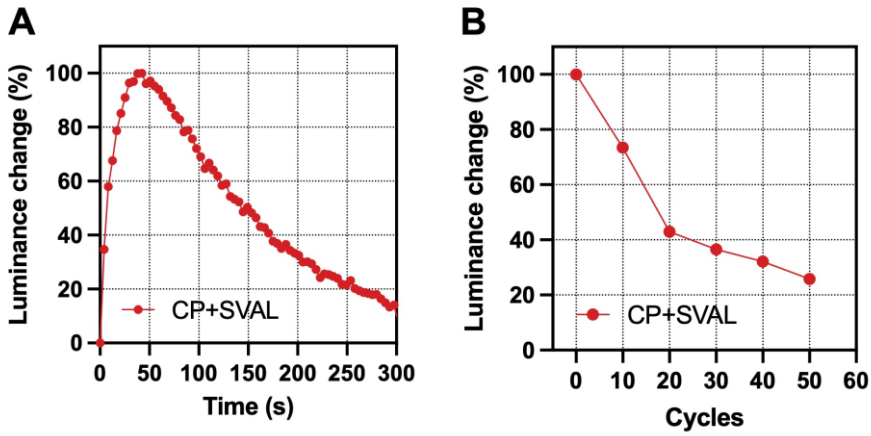

Figure 3.13. (A) Normalized luminance change of the ISOLED under a constant voltage of 8 V in air. (B) Variation of luminance of ISOLED with both CP and SVAL treatments at 8 V measured every 10 stretching cycles from 0 to 20% in air.

Table 3.1. Comparison of reported ISOLEDs

Ref	Device structure	V_{on} (V)	L_{max} (cd/m^2)	CE (cd/A)	Static stretching (chang in L, strain)
This work	TCSE/PEDOT:PSS/ SY:PEO:KCF_3SO_3/PEI/TCSE	3.7 (V_{on}) 2.7 (V_{th})	1754 (@11 V)	3.14	+4% (20%)
[19]	SWNT(PtBA)/PFB:PEO-DMA :LiTF/SWNT(PtBA)	~ 4.7	200 (@12 V)	0.76	−33% (20%)
[22]	AgNW(PUA)/PEDOT:PSS/SY:PEO :LiTF:ETPTA/PEI/AgNW(PUA)	6.8	2200 (@21 V)	11.4	+22% (20%)
[21]	AgNW(PUA)/PEDOT:PSS/OXD-7/PEI/AgNW(PUA)	7	1100 (@21 V)	4	-
[23]	AgNW(PDMS)/PEDOT:PSS/ SY:Triton X/PEI:ZnO:AgNW	8	4400 (@11 V)	1.6	+25% (20%)
[67]	Serpentine Au/Au/PEDOT:PSS/ L-SY-PPV-PAN/Zn-PEIE-pBphen-TR/Ag/AgNW/PDMS	6.5	3780 (@13 V)	2.35	−46% (30%)
[39]	PEDOT:PSS:Pr/PFN-Br:PEIE/SY:PU/TFB:PU PEDOT:PSS:TX/PEDOT:PSS:PR	5	7450 (@15 V)	5.3	+10% (25%)
[66]	TCSE/PEDOT:PSS/SY:TX /Crown-CPE/PEI/TCSE	5.3	2185 (@15 V)	20.3	-30% (20%)

Chapter 4. Titanium Carbide MXene-based Intrinsically Stretchable Phosphorescent Organic Light-Emitting Diodes with High Efficiency

4.1. Introduction

Intrinsically stretchable organic light-emitting diodes (ISOLEDs) that are attached to the human skin have been one of the most important media for visualization of the physiological signals obtained from the sensors.[20,65] Instead of rigid glass or silicon substrates, ISOLEDs were fabricated on elastomer substrates; this requires the materials used for ISOELD to endure large mechanical deformation.[66] However, strategies to improve stretchability will always degrade the electrical properties of the material, making the efficiency of the ISOLED far below their rigid counterparts with the same structure.[5] The low efficiency of the ISOLED severely hinders real-life applications in wearable electronics.[30]

One of the strategies to overcome this material paradox is to tune the charge transport and injection properties of stretchable electrodes such as conducting polymers and metal nanowire percolation networks.[66] Despite the excellent conductivity over 1000 s cm^{-1} and mechanical stretchability over 100% of PEDOT:PSS with the addition of secondary additives, the high work function of the PEDOT:PSS over 4.6 eV[65] limits its application for efficient electron injection. Besides, surface modification using polyethyleneimine (PEI) to reduce the work function will induce severe de-doping of the PEDOT, thereby significantly reducing the conductivity of the PEDOT:PSS electrode. Hence, metal nanowires such as silver nanowires (AgNWs) were used as the electrodes for the ISOLED.

AgNW percolation networks are normally embedded in the elastomer surface to

attain stretchability.[22] Nonetheless, the charge transport in the stretchable electrode can occur only along the wire, and the contact area between half-buried AgNW networks and the adjacent organic material is limited. Hence, charge transport and injection in stretchable electrodes that use AgNWs have been inefficient. To boost the efficiency of the ISOLED, we previously developed a two-dimensional contact stretchable electrode (TCSE) as both anode and cathode.[66] Graphene was introduced on the surface of embedded AgNW networks to form a two-dimensional contact with the organic material. The graphene interlayer significantly increased carrier mobility, work function tunability, and contact area of the TCSE, resulting in an improvement in the device current efficiency. However, CVD-grown graphene suffers from its poor solution processability and long process time for transferring process, making it less compatible with solution-processed devices. As an alternative, we have developed MXene as the two-dimensional contact layer for the stretchable AgNW electrode. High conductivity >10 000 S cm^{-1}, solution processibility, and its work function tunability (1.99 to 6.41 eV)[63], making it the best candidate electrode for the solution-processed ISOLEDs.

Herein we have developed MXene-based 2D contact stretchable electrodes for intrinsically stretchable phosphorescent organic light-emitting diodes (ISPhOLEDs). MXenes serve as the 2D interlayer to increase the electrical contact area without sacrificing the stretchability. The *WF* of MCSE can be successfully tuned from 3.79 to 5.71 eV for cathode and anode applications. Besides, we have also proposed a stretchable gradient hole injection layer to facilitate the hole injection with the addition of PFSA. In terms of the light-emitting layer, stretchability can be achieved with the addition of elastomer as the plasticizer. The intrinsically stretchable phosphorescent light-emitting device has been fabricated for the first time, and this

work will provide a guide for designing light-emitting devices in the future.

4.2. Materials and Experiments

The MXene solution was diluted to 4 mg/mL using the deionized water and the solution was left on the substrate for 3 min before spin-coating process. The waiting time allows the self-assembly of MXene flakes on the glass. The spin-coating process was carried out in two steps, once at 2000 rpm, 60 sec, and then at 6000 rpm for 90 sec. Then pristine AgNW solution (30 nm ×30 μm, Novarial, 5 mg/mL in isopropyl alcohol) as diluted to 2.5 mg/mL using IPA and spin-coated on top of as prepared MXene coated glass substrate. To bind the AgNW networks, 1 mg/mL MXene were used and spin-coated at 2000 rpm for 60 secs. The electrode was then transferred to the nitrogen filled glove box and heated at 150 ℃ for 12 h. Then the SEBS solution (180 mg/mL in toluene) was drop-cast on the electrode and kept overnight in air. The MCSE was then peeled off from the substrate in water. The A-MCSE was spin-coated using PFSA (2wt% in IPA) while the C-MCSE was prepared using PEI (3 wt% in 2-methoxyethanol).

For the preparation of SGraHIL, AI4083, PFI, and Zonyl was mixed based on the weight ratio of 1: 1.5:0.05. The SGraHIl was coated onto A-MCSE at 2000 rpm, 60 sec and heated at 90 ℃ for 10 min in air. Then to prepare the SPhEML, $Ir(ppy)_2acac$, TPBI and TAPC were mixed into elastomer solution at the concentration of 0.9, 5, and 5 mg/mL, respectively. A successive coating of SPhEML was performed at 3000 rpm, 60 sec in an N_2 filled glove box. The C-MCSE was then prepared with PEI coated at 3000 rpm, 60 sec and heated at 90 ℃ for 10 min. Crown-CPE was successively coated on C-MCSE to further reduce the work function. To perform the

lamination, the pressure of the hot pressing is finely tuned. The specimen was then hot pressed for 5 min in air.

Sheet resistance of MCSE was measured using a 4-point probe method. The transmittance of MCSE was measured using UV absorption spectroscopy (Lambda 465, PerkinElmer). The surface topographic and phase images were characterized using atomic force microscopy (NX-10, Park Systems). For static stretching tests, the strain was applied up to 100% by using a homemade setup operated with a stretching rate of 10 mm/min. The cyclic stretching test was conducted from $0 \leq$ strain $\leq$ 40% for 500 cycles repeatedly at a speed of 100 mm/min. *J–V–L* characteristics of ISOLEDs were measured using a spectroradiometer (CS2000, Konia Minolta) with a source meter.

4.3. Results and Discussion

SEBS was used as the elastomer for the MCSE due to its compatibility with the ligand of AgNW networks. MXene layer was formed on the surface of surface-embedded AgNW to increase the surface area of the MCSE (Figure 4.1A). Diluted MXene (1 mg/mL) was used as the binder to improve the interactions at the AgNW/AgNW and AgNW/MXene interfaces, resulting in enhanced electrical conductivity and mechanical stretchability(Figure 4.1B, C). With the incorporation of the surface modifier, the work function (*WF*) of the MCSE can be tuned either for anode (A-MCSE) or cathode (C-MCSE) applications. MCSE, A-MCSE, and C-MCSE showed low sheet resistance R_s of 29.9, 29.7, and 29.6 Ohm/sq, respectively.

Polyfluorosulfonic acid (PFSA) was used as the modifier to increase the work function of MCSE. The perfluoro backbone of PFSA had high ionization potential,

and the sulfonic group withdraws electrons from the MCSE electrode, thereby increasing the work function of MCSE to 5.71 eV and making it available as the A-MCSE. The combination of polyethyleneimine (PEI) and crown-conjugated polyelectrolyte (Crown-CPE) was introduced onto the surface of MCSE. The strong interfacial dipole of PEI has significantly reduced the *WF* of pristine MCSE from 4.73 to 3.99 eV. Due to the hydrogen bonding interaction between the crown ether group of Crown-CPE and amine groups of PEI, CPE forms self-assembled moieties on the surface of MCSE; this further reduces the *WF* to 3.79 eV (Figure 4.1D).

To make the MCSE available for the successive solution process, controlling the *d*-spacing of MXene is important. Due to the intercalation of Li ions between the MXene layer, fast hydration of Li ions enlarges the *d*-spacing of MXene and degrades the electrical conductivity of the MXene electrode.[63] Hence, MXene is vulnerable to the solution process. To increase the resistance of MXene against moisture, the *d*-spacing of MXene can be significantly reduced using a low-temperature annealing process. Even though high-temperature annealing can further reduce the *d*-spacing of MXene, high-temperature annealing over 200 ℃ can significantly enhance the adhesion between MXene and substrates; this makes the surface embedding process challenging. Hence, low-temperature annealing was carried out at 150 ℃, and the variation of MXene *d*-spacing can be characterized using X-ray diffraction (XRD). Compared with the pristine MXene without any treatment, the diffraction peak of MXene in the MCSE increased from 7.42 to 7.96º (Figure 4.2A); this corresponds to a reduction of d-spacing from 1.19 to 1.11 nm (Figure 4.2B). Both pristine MXene and MCSE were tested for solution stability with the contact protected by the copper tape to minimize the effect of the contact resistance caused by the PEDOT:PSS solution. Pristine MXene showed a significant

reduction in conductivity after PEDOT:PSS coating (Figure 4.2C), whereas the slope of MCSE did not show any changes (Figure 4.2D); this proves the enhanced stability of MXene against moisture.

Then the mechanical stretchability of MCSE was evaluated using a homemade stretcher. When compared with the AgNW electrode without any additional treatments, the resistance change (defined by the resistance of the electrode after stretching to the initial resistance, R/R_0) MCSE electrode showed a resistance change of 1.42 at 20% of strain, whereas that value of AgNW was as large as 3.09 at the same strain (Figure 4.3A). At higher strains, the stability of MCSE was superior to that of AgNW due to MXene 2D contact and the MXene binder. In the cyclic stretching test at 40% strain, superior mechanical stretchability of MXene can also be observed (Figure 4.3B). The MXene 2D contact contributes to the difference in mechanical stretchability. AgNW functions as the bridge to connect the cracks under stretching, forming an "island-bridge" structure (Figure 4.3C). The conduction path, therefore, can be maintained even under stretching.

Then, the stretchable hole injection layer of the stretchable phosphorescent layer was characterized. We have proposed a new concept named stretchable gradient hole injection layer (SGraHIL). To increase the stretchability of the hole injection layer, surfactant was added to PEDOT:PSS to induce phase separation between PEDOT and PSS and aggregated soft PSS domain significantly increases the stretchability of the PEDOT:PSS. The conventional stretchable hole injection layer was composed of PEDOT:PSS with 5 wt% of Triton X, whereas in the SGraHIL, Zonyl FS-300 and PFSA were added to enhance the stretchability, and the work function, respectively (Figure 4.4A). Because of the low surface energy of PFSA, it tends to form a concentration gradient with high surface PFSA content. Due to the perfluoro

backbone of PFSA, the *WF* of SGraHIL was significantly enhanced to 5.65 eV, whereas the SHIL showed a low *WF* of 4.61 eV (Figure 4.4B). The high *WF* of SGraHIL is beneficial to efficient hole injection.

In addition, due to the high electrical conductivity of the PEDOT:PSS surface, exciton quenching is another important issue that needs to be solved on the SHIL surface.[24] The SHIL exhibited strong exciton quenching, whereas the PL intensity of the stretchable light-emitting layer coated on SGraHIL is substantially higher (Figure 4.4C), indicating the high insulating PFSA content on the surface. To prove the existence of a PFSA concentration gradient, TOF-SIMS analysis was conducted to analyze the variation of elements (Figure 4.4D,E). The SHIL showed a sharp decrease in all elements when the sampling surface is getting closer to the substrate surface. However, the PFSA in the SGraHIL declined faster than that of other groups, implying that the PFSA content near the substrate surface is lower. Hence, it is sufficient to prove that PFSA forms a concentration gradient from the substrate to the surface of SGraHIL. Due to the phase separation with the addition of Zonyl FS-300, the SGraHIL can be successfully stretched without forming any cracks under 40% of strain (Figure 4.4F).

The next layer that needs to be optimized is the stretchable phosphorescent light-emitting layer (SPhEML). Compared to the fluorescent light-emitting polymer, we used phosphorescent light-emitting materials to use it for stretchable application. Tris(4-carbazoyl-9-ylphenyl)amine (TCTA) and 2,2',2''-(1,3,5-Benzinetriyl)-tris(1-phenyl-1-H-benzimidazole) (TPBi) were used as the mixed host for the bis[2-(2-pyridinyl-N)phenyl-C](acetylacetonato)iridium(III)($Ir(ppy)_2(acac)$) (Figure 4.5A). Due to its low solubility, the concentration of the dopant in THF solution is limited to 1 mg/mL. To increase the stretchability of the SEML, we added PU or SEBS as

the plasticizer to enhance the stretchability. Since SEBS does not contain any polar groups, its miscibility with light-emitting materials with substantially lower than that of PU. Hence with increasing PU content, exciton quenching induced by the dopant aggregation is suppressed, leading to an increase in PL intensity. But an opposite trend was observed in the case of SEBS (Figure 4.5B). The change in PL intensity can be seen from the photographs of the SPhEML using SEBS or PU (Figure 4.5C). With increasing PU content, the film coated on the substrate became brighter while in the case of SEBS, the brightness remained at the same level. To explain the difference in the PL intensity, we have characterized the PL lifetime using the transient PL. Hence, the increase in PL in PU from 1.36 (0%) to 1.45 μs (40%) indicates that PL quenching can be suppressed because of the PU matrix (Figure 4.5D). Finally, the film with different elastomer content was characterized using atomic force microscopy (AFM) (Figure 4.5E). Clear phase separation between the light-emitting layer and the SEBS can be seen with the addition of SEBS. While due to the hydrophilicity of PU, the composite light-emitting layer forms a uniform film.

To check the feasibility of the MCSE/SGraHIL/SPhEML structure, the device with deposited with TPBi/LiF/Al for efficient electron injection (Figure 4.6A). When compared with the ITO-based device, MCSE showed a similar charge injection capability with a threshold voltage of around 4 V (Figure 4.6B). The turn-on voltage of both devices was similar at 4.5 V, with the maximum luminance around 2300 cd/m^2 (Figure 4.6C). The maximum current efficiency of ITO at 43 cd/A is slightly higher than that of an MCSE-based device at 40 cd/A (Figure 4.6D). Finally, the ISPhOLED was fabricated using the lamination method. The C-MCSE with Crown-CPE was formed on another substrate and then attached to the SPhEML by applying heat and pressure (Figure 4.7). The maximum current efficiency of the SPhEML is

around 10 cd/A and the optimization is still in progress. But it is sufficient to prove that the device architecture functions well and can be applied to stretchable light-emitting devices with high efficiency.

4.4. Conclusion

In this work, we have developed MXene-based 2D contact stretchable electrodes for intrinsically stretchable phosphorescent organic light-emitting diodes (ISPhOLEDs). MXenes serve as the 2D interlayer to increase the electrical contact area without sacrificing the stretchability. The *WF* of MCSE can be successfully tuned from 3.79 to 5.71 eV for cathode and anode applications. Besides, we have also proposed a stretchable gradient hole injection layer to facilitate the hole injection with the addition of PFSA. In terms of the light-emitting layer, stretchability can be achieved with the addition of elastomer as the plasticizer. The intrinsically stretchable phosphorescent light-emitting device has been fabricated for the first time, and this work will provide a guide for designing light-emitting devices in the future.

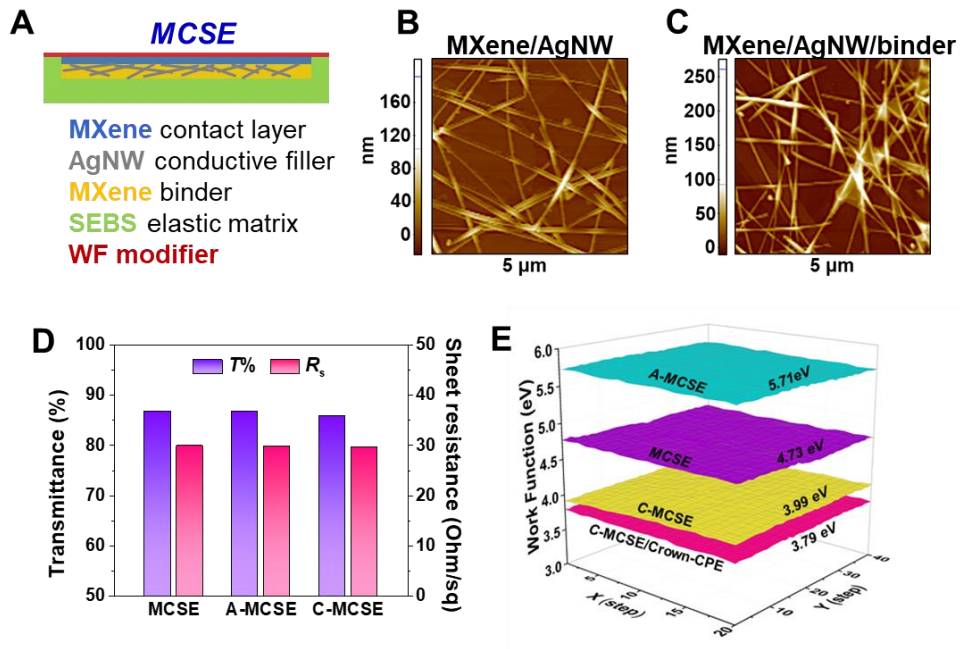

Figure 4.1. (A) Conceptual illustration of the MXene contact stretchable electrode (MCSE) that consists of MXene contact layer, AgNW conductive filler, MXene binder, SEBS elastomeric matrix and a layer of work function modifier. (B) and (C) AFM topography of MXene AgNW before and after welding process using MXene solution. (D) Transmittance and sheet resistance of MCSE, MCSE with high *WF* as the anode (A-MCSE), and MCSE with low *WF* as the cathode (C-MCSE). (E) Kelvin probe mapping of *WF* of A-MCSE, MCSE, C-MCSE and C-MCSE/Crown-CPE.

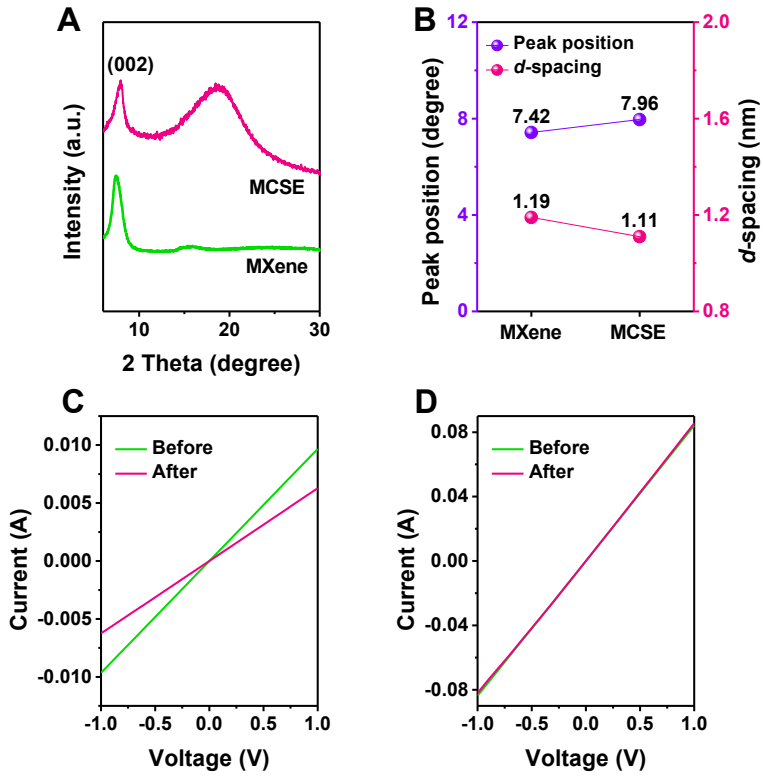

Figure 4.2. (A) XRD patterns showing the dominant (002) out-of-plane reflection. (B) XRD peak positions extracted from (A) and *d*-spacing calculated based on Bragg's law. (C) and (D) Current *vs.* voltage curves before and after coating with PEDOT:PSS, respectively.

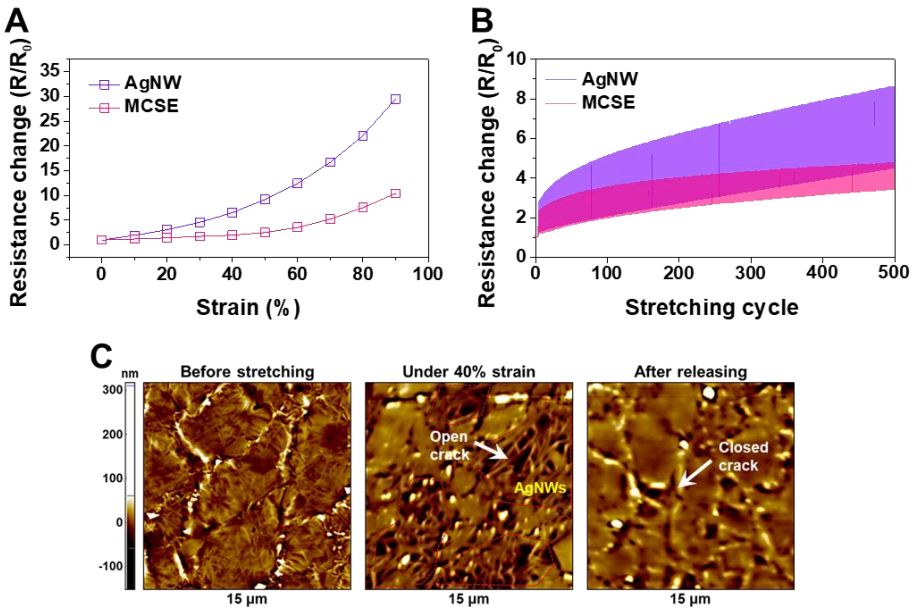

Figure 4.3. (A) and (B) Static and cyclic stretching tests (strain = 40%) of AgNW, MCSE (C) Atomic force microscopy (AFM) phase images taken during the *in-situ* stretching test (strain = 40%) on MXene that had been transferred onto SEBS.

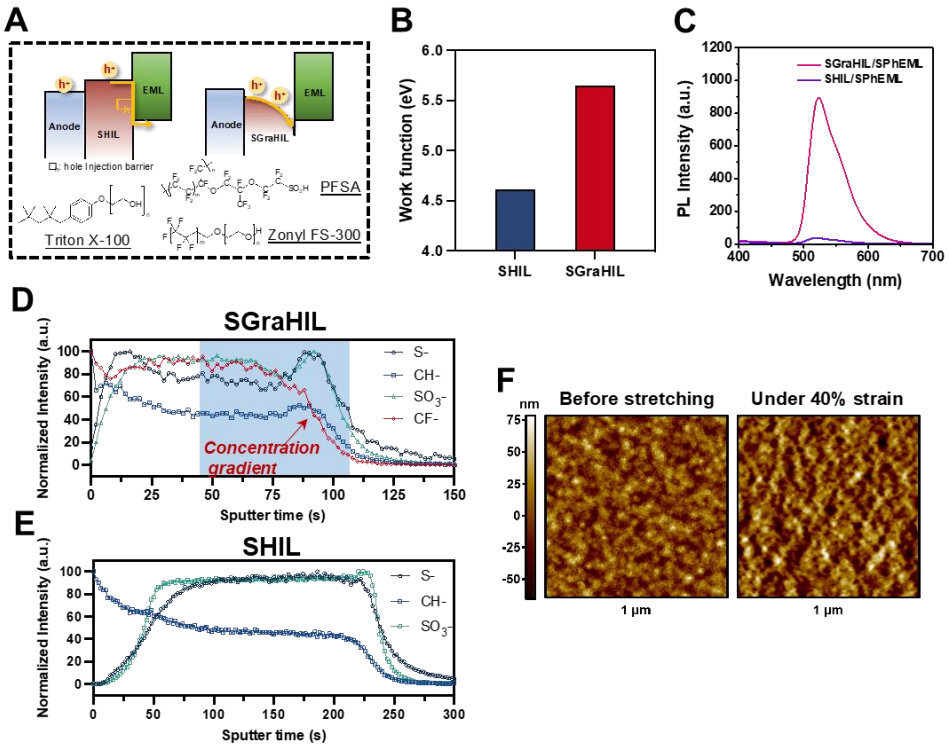

Figure 4.4. (A) Composition of SHIL and SGraHIL and schematic illustration of their band structures. (B) Work function of SHIL and SGraHIL measured using Kelvin Probe. (C) The PL spectrum of the stretchable phosphorescent light-emitting layer (SPhEML) on SHIL and SGraHIL, respectively. (D) and (E) TOF-SIMS analysis on SGraHIL, and SHIL, respectively. (F) AFM topography images taken during the *in-situ* stretching test (strain = 40%) on SGraHIL.

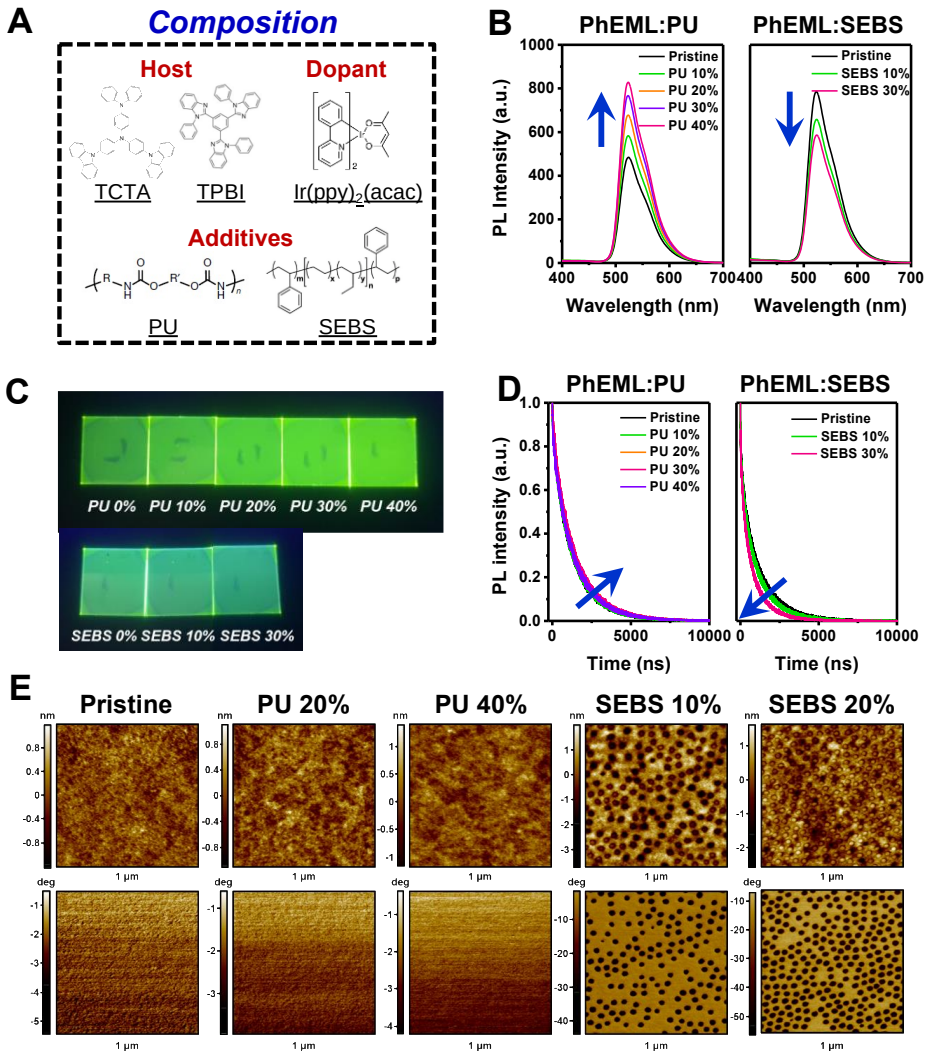

Figure 4.5. (A) Components of SPhEML with SEBS or PU as the polymer matrix. (B) Variation of PL spectrum, (C) digital images, and (D) transient PL of SPhEML with addition of increasing amount of PU or SEBS. (E) AFM topography and phase images of SPhEML with addition of varying elastomer content.

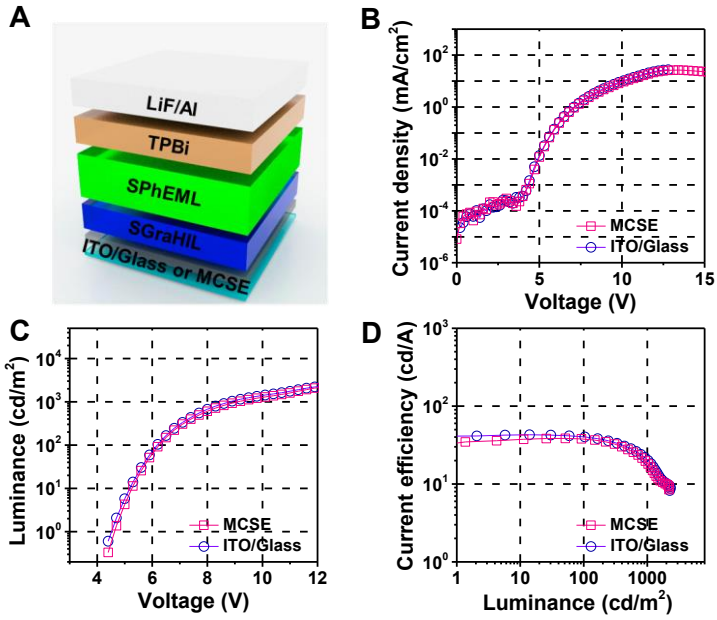

Figure 4.6. (A) Schematic illustration of device architecture. ITO or MCSE/SGraHIL/SPhEML/TPBI/LiF/Al. (B) Current density vs. voltage, (C) luminance vs. voltage and (D) current efficiency vs. luminance characteristics of the MCSE and ITO-based devices.

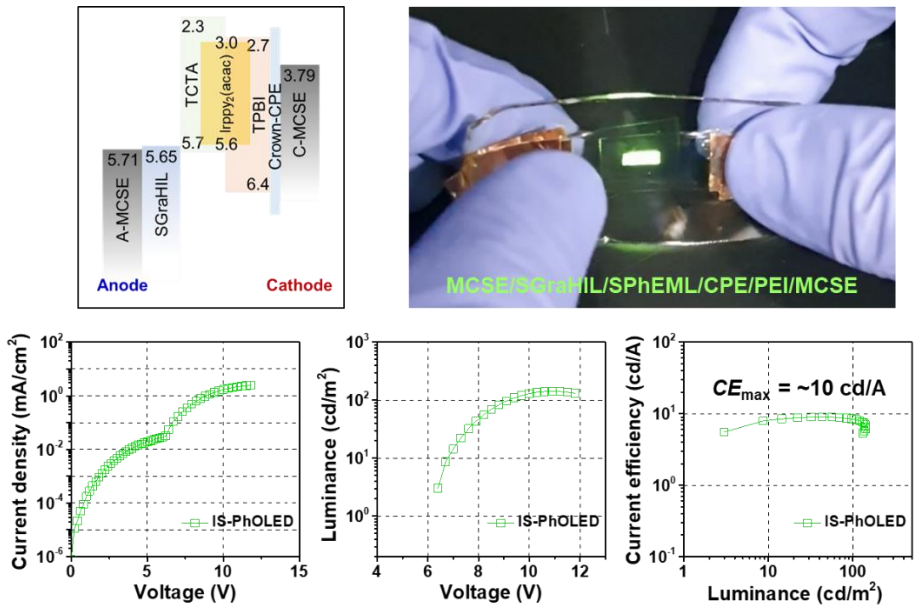

Figure 4.7. (A) Band diagram (B) digital image of ISPhOLED. (C) Current density vs. voltage, (D) luminance vs. voltage and (E) current efficiency vs. luminance characteristics ISPhOLED.

Chapter 5. Summary

The development of intrinsically-stretchable organic light-emitting didoes (ISOLEDs) has stagnated due to the lack of ideal stretchable electrode materials to overcome the existing issue of poor charge injection at the electrode interface, and consequent high turn-on voltage V_{on} > 7 V, although the stretchability has been improved significantly. Herein, we present a two-dimensional-contact stretchable electrode (TCSE) that consists of AgNWs as the conductive filler, two-dimensional graphene as the work function (*WF*) modifier on the surface, GO binder to enhance conductivity and stretchability, and dopants to control the *WF*. The *WF* of the TCSE can be modulated to 5.69 eV and 4.04 eV by *p*- and *n*-type doping, respectively. TCSE can fulfill the required energy-level alignment with reduced the charge-injection barrier and form a two-dimensional electrical contact with the adjacent organic layer upon lamination for efficient charge injection. An ISOLED using the laminated doped TCSE exhibited low V_{on} of 5.5 V, maximum luminance (L_{max}) of 1130 cd/m^2, current efficiency (CE) of 9.3 cd/A, and a stable light-emission with LT_{50} = 7.07h (the lifetime at 50% initial luminance under continuous operation). Furthermore, we demonstrated a three-inch five-by-five passive matrix ISOLED using the convex stretching method.

To further develop the practical applications of intrinsically stretchable optoelectronic devices with enhanced performances, a new lamination method has been introduced to obtain a uniform lamination contact and strong adhesion at the interface. A minimum operating voltage of intrinsically stretchable organic light-emitting diodes (ISOLEDs) is required for practical applications. However, the absence of lamination standards has significantly retarded the field of ISOLEDs,

making it extremely challenging to attain reliable ISOLEDs. In this work, we present a holistic protocol to reinforce a weakly laminated cathode interface in ISOLEDs, thereby simultaneously increasing the mechanical stretchability and lowering the operating voltage. Achieving a uniform contact and strong adhesion at the interface are the prerequisites to attaining a reliable laminated interface. A cold-pressing (CP) treatment was first introduced to reduce the surface roughness of silver nanowires of the stretchable electrode before the embedding process. The subsequent solvent-vapor assisted lamination (SVAL) partially solvates the surface of the light-emitting layer with an increase in the segmental motion of polymer chains, which substantially increases the interfacial adhesion at the interface. These benefits from a combination of CP and SVAL treatments substantially reduced threshold voltage V_{th} from 6.7 to 2.7 V. The ISOLED also exhibits excellent mechanical stretchability, with no significant change in luminance under 30% strain.

CVD-grown graphene suffers from its poor solution processability and long process time for transferring process, making it less compatible with solution-processed devices. To simplify the process of the two-dimensional contact stretchable electrode, we have introduced MXene as the two-dimensional contact layer for the stretchable AgNW electrode instead of graphene. MXene is a fast-growing material having two-dimensional structure for optoelectronic devices owing to its attractive properties such as *WF* modulating capabilities, metallic conductivity, and solution processability with hydrophilic groups on the surface. Herein we demonstrate MXene-based 2D contact stretchable electrodes for intrinsically stretchable phosphorescent organic light-emitting diodes (ISPhOLEDs). MXenes serve as the 2D interlayer to increase the electrical contact area without sacrificing the stretchability. The *WF* of MCSE can be successfully tuned from 3.79 to 5.71 eV

for cathode and anode applications. Besides, we have also proposed a stretchable gradient hole injection layer to facilitate the hole injection with the addition of PFSA. In terms of the light-emitting layer, stretchability can be achieved with the addition of elastomer as the plasticizer. Lastly, the intrinsically stretchable phosphorescent light-emitting device with the high efficiency has been fabricated for the first time.

This dissertation can provide effective guidelines for designing two-dimensional contactable stretchable electrodes with 2D materials and intrinsically stretchable organic light-emitting diodes with high efficiency.

Bibliography

[1] Liu, Y., Xiao, H., and Goddard, W. A. *J. Am. Chem. Soc.* **2016**, 138, 15853.

[2] Bauer, S. *Nature Materials* **2013**, 12, 871.

[3] Someya, T., and Amagai, M. *Nat. Biotechnol.* **2019**, 37, 382.

[4] Chen, D., and Pei, Q. *Chemical Reviews* **2017**, 117, 11239.

[5] Zhou, H., Park, J., Lee, Y., Park, J.-M., Kim, J.-H., Kim, J. S., Lee, H.-D., Jo, S. H., Cai, X., Li, L., Sheng, X., Yun, H. J., Park, J.-W., Sun, J.-Y., and Lee, T.-W. *Adv. Mater.* **2020**, 32, 2001989.

[6] Chu, B., Burnett, W., Chung, J. W., and Bao, Z. *Nature* **2017**, 549, 328.

[7] Qian, Y., Zhang, X., Xie, L., Qi, D., Chandran, B. K., Chen, X., and Huang, W. *Advanced Materials* **2016**, 28, 9243.

[8] Rogers, J. A., Someya, T., and Huang, Y. *Science* **2010**, 327, 1603.

[9] Oh, J. Y., and Bao, Z. *Adv. Sci.* **2019**, 6, 1900186.

[10] Wang, B., and Facchetti, A. *Adv. Mater.* **2019**, 31, 1901408.

[11] Wang, C., Wang, C., Huang, Z., and Xu, S. *Adv. Mater.* **2018**, 30, 1801368.

[12] Yin, H., Zhu, Y., Youssef, K., Yu, Z., and Pei, Q. *Adv. Mater.*, n/a, 2106184.

[13] Wang, Y., Zhu, C., Pfattner, R., Yan, H., Jin, L., Chen, S., Molina-Lopez, F.,

Lissel, F., Liu, J., Rabiah, N. I., Chen, Z., Chung, J. W., Linder, C., Toney, M. F., Murmann, B., and Bao, Z. *Science Advances* **2017**, 3, e1602076.

[14] Xu, J., Wang, S., Wang, G.-J. N., Zhu, C., Luo, S., Jin, L., Gu, X., Chen, S., Feig, V. R., To, J. W. F., Rondeau-Gagné, S., Park, J., Schroeder, B. C., Lu, C., Oh, J. Y., Wang, Y., Kim, Y.-H., Yan, H., Sinclair, R., Zhou, D., Xue, G., Murmann, B., Linder, C., Cai, W., Tok, J. B.-H., Chung, J. W., and Bao, Z. *Science* **2017**, 355, 59.

[15] Dinh Xuan, H., Timothy, B., Park, H.-Y., Lam, T. N., Kim, D., Go, Y., Kim, J., Lee, Y., Ahn, S. I., Jin, S.-H., and Yoon, J. *Adv. Mater.* **2021**, 33, 2008849.

[16] Li, S., Peele, B. N., Larson, C. M., Zhao, H., and Shepherd, R. F. *Adv. Mater.* **2016**, 28, 9770.

[17] Wang, J., Yan, C., Chee, K. J., and Lee, P. S. *Adv. Mater.* **2015**, 27, 2876.

[18] Zhang, Z., Guo, K., Li, Y., Li, X., Guan, G., Li, H., Luo, Y., Zhao, F., Zhang, Q., Wei, B., Pei, Q., and Peng, H. *Nat. Photonics* **2015**, 9, 233.

[19] Zhibin, Y., Xiaofan, N., Zhitian, L., and Qibing, P. *Adv. Mater.* **2011**, 23, 3989.

[20] Liu, J., Wang, J., Zhang, Z., Molina-Lopez, F., Wang, G.-J. N., Schroeder, B. C., Yan, X., Zeng, Y., Zhao, O., Tran, H., Lei, T., Lu, Y., Wang, Y.-X., Tok, J. B. H., Dauskardt, R., Chung, J. W., Yun, Y., and Bao, Z. *Nature Communications* **2020**, 11, 3362.

[21] Liang, J., Li, L., Tong, K., Ren, Z., Hu, W., Niu, X., Chen, Y., and Pei, Q.

ACS Nano **2014**, 8, 1590.

[22] Liang, J., Li, L., Niu, X., Yu, Z., and Pei, Q. *Nat. Photonics* **2013**, 7, 817.

[23] Kim, J. H., and Park, J. W. *Sci. Adv.* **2021**, 7, eabd9715.

[24] Han, T.-H., Lee, Y., Choi, M.-R., Woo, S.-H., Bae, S.-H., Hong, B. H., Ahn, J.-H., and Lee, T.-W. *Nat. Photonics* **2012**, 6, 105.

[25] Kwon, S.-J., Han, T.-H., Ko, T. Y., Li, N., Kim, Y., Kim, D. J., Bae, S.-H., Yang, Y., Hong, B. H., Kim, K. S., Ryu, S., and Lee, T.-W. *Nat. Commun.* **2018**, 9, 2037.

[26] Ahn, S., Han, T.-H., Maleski, K., Song, J., Kim, Y.-H., Park, M.-H., Zhou, H., Yoo, S., Gogotsi, Y., and Lee, T.-W. *Adv. Mater.* **2020**, 32, 2000919.

[27] Helander, M. G., Wang, Z. B., Qiu, J., Greiner, M. T., Puzzo, D. P., Liu, Z. W., and Lu, Z. H. *Science* **2011**, 332, 944.

[28] Iqbal, A., Shahzad, F., Hantanasirisakul, K., Kim, M.-K., Kwon, J., Hong, J., Kim, H., Kim, D., Gogotsi, Y., and Koo, C. M. *Science* **2020**, 369, 446.

[29] Zhou, Y., Fuentes-Hernandez, C., Shim, J., Meyer, J., Giordano, A. J., Li, H., Winget, P., Papadopoulos, T., Cheun, H., Kim, J., Fenoll, M., Dindar, A., Haske, W., Najafabadi, E., Khan, T. M., Sojoudi, H., Barlow, S., Graham, S., Bredas, J. L., Marder, S. R., Kahn, A., and Kippelen, B. *Science* **2012**, 336, 327.

[30] Yin, H., Zhu, Y., Youssef, K., Yu, Z., and Pei, Q. *Adv. Mater.* **2021**, 2106184.

[31] Lee, S., Sasaki, D., Kim, D., Mori, M., Yokota, T., Lee, H., Park, S., Fukuda, K., Sekino, M., Matsuura, K., Shimizu, T., and Someya, T. *Nat. Nanotechnol.* **2019**, 14, 156.

[32] Lee, Y., Chung, J. W., Lee, G. H., Kang, H., Kim, J.-Y., Bae, C., Yoo, H., Jeong, S., Cho, H., Kang, S.-G., Jung, J. Y., Lee, D.-W., Gam, S., Hahm, S. G., Kuzumoto, Y., Kim, S. J., Bao, Z., Hong, Y., Yun, Y., and Kim, S. *Sci. Adv.* **2021**, 7, eabg9180.

[33] You, I., Mackanic, D. G., Matsuhisa, N., Kang, J., Kwon, J., Beker, L., Mun, J., Suh, W., Kim, T. Y., Tok, J. B.-H., Bao, Z., and Jeong, U. *Science* **2020**, 370, 961.

[34] Matsuhisa, N., Niu, S., O'Neill, S. J. K., Kang, J., Ochiai, Y., Katsumata, T., Wu, H.-C., Ashizawa, M., Wang, G.-J. N., Zhong, D., Wang, X., Gong, X., Ning, R., Gong, H., You, I., Zheng, Y., Zhang, Z., Tok, J. B. H., Chen, X., and Bao, Z. *Nature* **2021**, 600, 246.

[35] Son, D., Kang, J., Vardoulis, O., Kim, Y., Matsuhisa, N., Oh, J. Y., To, J. W. F., Mun, J., Katsumata, T., Liu, Y., McGuire, A. F., Krason, M., Molina-Lopez, F., Ham, J., Kraft, U., Lee, Y., Yun, Y., Tok, J. B. H., and Bao, Z. *Nature Nanotechnology* **2018**.

[36] Larson, C., Peele, B., Li, S., Robinson, S., Totaro, M., Beccai, L., Mazzolai, B., and Shepherd, R. *Science* **2016**, 351, 1071.

[37] Tan, Y. J., Godaba, H., Chen, G., Tan, S. T. M., Wan, G., Li, G., Lee, P. M.,

Cai, Y., Li, S., Shepherd, R. F., Ho, J. S., and Tee, B. C. K. *Nature Materials* **2020**, 19, 182.

[38] Shi, X., Zuo, Y., Zhai, P., Shen, J., Yang, Y., Gao, Z., Liao, M., Wu, J., Wang, J., Xu, X., Tong, Q., Zhang, B., Wang, B., Sun, X., Zhang, L., Pei, Q., Jin, D., Chen, P., and Peng, H. *Nature* **2021**, 591, 240.

[39] White, M. S., Kaltenbrunner, M., Głowacki, E. D., Gutnichenko, K., Kettlgruber, G., Graz, I., Aazou, S., Ulbricht, C., Egbe, D. A. M., Miron, M. C., Major, Z., Scharber, M. C., Sekitani, T., Someya, T., Bauer, S., and Sariciftci, N. S. *Nat. Photonics* **2013**, 7, 811.

[40] Cheng, T., Zhang, Y., Lai, W. Y., and Huang, W. *Advanced Materials* **2015**, 27, 3349.

[41] Li, D., Lai, W. Y., Zhang, Y. Z., and Huang, W. *Advanced materials* **2018**, 30, 1704738.

[42] Höfle, S., Schienle, A., Bruns, M., Lemmer, U., and Colsmann, A. *Advanced Materials* **2014**, 26, 2750.

[43] Maiti, U. N., Lee, W. J., Lee, J. M., Oh, Y., Kim, J. Y., Kim, J. E., Shim, J., Han, T. H., and Kim, S. O. *Adv. Mater.* **2014**, 26, 40.

[44] Loh, K. P., Bao, Q., Eda, G., and Chhowalla, M. *Nature Chemistry* **2010**, 2, 1015.

[45] Liu, Y., Zhang, J., Gao, H., Wang, Y., Liu, Q., Huang, S., Guo, C. F., and Ren, Z. *Nano Lett.* **2017**, 17, 1090.

[46] Dikin, D. A., Stankovich, S., Zimney, E. J., Piner, R. D., Dommett, G. H. B., Evmenenko, G., Nguyen, S. T., and Ruoff, R. S. *Nature* **2007**, 448, 457.

[47] Ferrari, A. C., and Basko, D. M. *Nature Nanotechnology* **2013**, 8, 235.

[48] Nicholl, R. J. T., Conley, H. J., Lavrik, N. V., Vlassiouk, I., Puzyrev, Y. S., Sreenivas, V. P., Pantelides, S. T., and Bolotin, K. I. *Nature Communications* **2015**, 6, 8789.

[49] Liu, N., Chortos, A., Lei, T., Jin, L., Kim, T. R., Bae, W.-G., Zhu, C., Wang, S., Pfattner, R., Chen, X., Sinclair, R., and Bao, Z. *Sci. Adv.* **2017**, 3, e1700159.

[50] Ahn, Y., Jeong, Y., and Lee, Y. *ACS Appl. Mater. Interfaces* **2012**, 4, 6410.

[51] Kusoglu, A., and Weber, A. Z. *Chemical Reviews* **2017**, 117, 987.

[52] Lee, Y., Zhou, H., and Lee, T.-W. *Journal of Materials Chemistry C* **2018**, 6, 3538.

[53] Wang, C., Hwang, D., Yu, Z., Takei, K., Park, J., Chen, T., Ma, B., and Javey, A. *Nat. Mater.* **2013**, 12, 899.

[54] Zhou, H., and Lee, T.-W. *IEEE Spectrum* **2020**, 57, 24.

[55] Zhou, H., Han, S. J., Lee, H.-D., Zhang, D., Anayee, M., Jo, S. H., Gogotsi, Y., and Lee, T.-W. *Adv. Mater.* **2022**, 2206377.

[56] Yin, D., Jiang, N.-R., Chen, Z.-Y., Liu, Y.-F., Bi, Y.-G., Zhang, X.-L., Feng,

J., and Sun, H.-B. *Adv. Opt. Mater.* **2020**, 8, 1901525.

[57] Lim, M. S., Nam, M., Choi, S., Jeon, Y., Son, Y. H., Lee, S.-M., and Choi, K. C. *Nano Lett.* **2020**, 20, 1526.

[58] Choi, D. K., Kim, D. H., Lee, C. M., Hafeez, H., Sarker, S., Yang, J. S., Chae, H. J., Jeong, G.-W., Choi, D. H., Kim, T. W., Yoo, S., Song, J., Ma, B. S., Kim, T.-S., Kim, C. H., Lee, H. J., Lee, J. W., Kim, D., Bae, T.-S., Yu, S. M., Kang, Y.-C., Park, J., Kim, K.-H., Sujak, M., Song, M., Kim, C.-S., and Ryu, S. Y. *Nat. Commun.* **2021**, 12, 2864.

[59] Yin, D., Feng, J., Ma, R., Liu, Y.-F., Zhang, Y.-L., Zhang, X.-L., Bi, Y.-G., Chen, Q.-D., and Sun, H.-B. *Nat. Commun.* **2016**, 7, 11573.

[60] Yokota, T., Zalar, P., Kaltenbrunner, M., Jinno, H., Matsuhisa, N., Kitanosako, H., Tachibana, Y., Yukita, W., Koizumi, M., and Someya, T. *Sci. Adv.* **2016**, 2, e1501856.

[61] Son, D., Kang, J., Vardoulis, O., Kim, Y., Matsuhisa, N., Oh, J. Y., To, J. W., Mun, J., Katsumata, T., Liu, Y., McGuire, A. F., Krason, M., Molina-Lopez, F., Ham, J., Kraft, U., Lee, Y., Yun, Y., Tok, J. B., and Bao, Z. *Nature Nanotechnology* **2018**, 13, 1057.

[62] Park, J.-M., Park, J., Kim, Y.-H., Zhou, H., Lee, Y., Jo, S. H., Ma, J., Lee, T.-W., and Sun, J.-Y. *Nature Communications* **2020**, 11, 4638.

[63] Zhou, H., Han, S. J., Lee, H.-D., Zhang, D., Anayee, M., Jo, S. H., Gogotsi, Y., and Lee, T.-W. *Adv. Mater.* **2022**, 34, 2270288.

[64] Liang, J., Li, L., Tong, K., Ren, Z., Hu, W., Niu, X., Chen, Y., and Pei, Q. *ACS Nano* **2014**, 8, 1590.

[65] Zhang, Z., Wang, W., Jiang, Y., Wang, Y.-X., Wu, Y., Lai, J.-C., Niu, S., Xu, C., Shih, C.-C., Wang, C., Yan, H., Galuska, L., Prine, N., Wu, H.-C., Zhong, D., Chen, G., Matsuhisa, N., Zheng, Y., Yu, Z., Wang, Y., Dauskardt, R., Gu, X., Tok, J. B. H., and Bao, Z. *Nature* **2022**, 603, 624.

[66] Zhou, H., Han, S. J., Harit, A. K., Kim, D. H., Kim, D. Y., Choi, Y. S., Kwon, H., Kim, K. N., Go, G. T., Yun, H. J., Hong, B. H., Suh, M. C., Ryu, S. Y., Woo, H. Y., and Lee, T. W. *Adv. Mater.* **2022**, 34, 2203040.

[67] Liu, Y., Zhu, M., Sun, J., Shi, W., Zhao, Z., Wei, X., Huang, X., Guo, Y., and Liu, Y. *Adv. Mater.* **2022**, 34, 2201844.

[68] Zhou, H., and Park, J.-W. *Org. Electron.* **2015**, 24, 272.

[69] Zhou, H., and Park, J.-W. *Thin Solid Films* **2016**, 619, 281.

[70] Zhou, H., Han, S. J., Harit, A. K., Kim, D. H., Kim, D. Y., Choi, Y. S., Kwon, H., Kim, K.-N., Go, G.-T., Yun, H. J., Hong, B. H., Suh, M. C., Ryu, S. Y., Woo, H. Y., and Lee, T.-W. *Adv. Mater.* **2022**, 34, 2270228.

[71] Cabrerizo, F. M., Arnbjerg, J., Denofrio, M. P., Erra-Balsells, R., and Ogilby, P. R. *ChemPhysChem* **2010**, 11, 796.

[72] Lei, T., Dou, J.-H., Cao, X.-Y., Wang, J.-Y., and Pei, J. *J. Am. Chem. Soc.* **2013**, 135, 12168.

[73] Brown, T. M., Friend, R. H., Millard, I. S., Lacey, D. J., Burroughes, J. H., and Cacialli, F. *Appl. Phys. Lett.* **2000**, 77, 3096.

[74] Gao, H., Chen, S., Liang, J., and Pei, Q. *ACS Appl. Mater. Interfaces* **2016**, 8, 32504.

[75] Sawyer, E. J., Zaretski, A. V., Printz, A. D., de los Santos, N. V., Bautista-Gutierrez, A., and Lipomi, D. J. *Extreme Mechanics Letters* **2016**, 8, 78.

Curriculum Vitae

Education & Training

2019.03– 2023.02	Ph.D. in Department of Materials Science and Engineering, Seoul National University (Advisor: Prof. Tae-Woo Lee)
2005.03– 2007.02	M.S. in Department of Materials Science and Engineering, Seoul National University (Advisor: Prof. Seung-Yeop Kwak) Thesis: *Synthesis of Mesoporous TiO_2 with Various Pore Size Distributions and Characterization of Their Photocatalytic Activity*
1999.03– 2005.02	B.S. in Department of Textile System Engineering, Kyungpook National University

Work Experience

2007.02- 2008.08	Samsung SDI, LCD/OLED division
2008.09- 2012.03	Samsung Mobile Display, OLED division
2012.04-	Samsung Display, OLED division

Publications

1. H. Zhou+, **S. J. Han+**, A. K. Harit+ (+: equally contributed to this work), D. H. Kim, D. Y. Kim, Y. S. Choi, H. Kwon, K. -N. Kim, G. -T. Go, H. J. Yun, B. H. Hong, S. Y. Ryu, M. C. Suh, H. Y. Woo* and T.-W. Lee* "Graphene-based Intrinsically Stretchable Two-Dimensional-Contact Electrodes for Highly Efficient Organic Light-Emitting Diodes", ***Advanced Materials,*** 2022, 34, 2203040 (**Featured as frontispiece**)

2. H. Zhou+, **S. J. Han+**, H. -D. Lee+ (+: equally contributed to this work), D. Zhang, M. Anayee, Y. Gogotsi*, and T.-W. Lee* "Overcoming the Limitations of MXene Electrodes for Solution-Processed Optoelectronic Devices", ***Advanced Materials,*** 2022, 34, 2206377

3. **S. J. Han+**, H. Zhou+ (+: equally contributed to this work), H. Kwon, S. –J. Woo, T. –W. Lee* "Achieving Low-Voltage Operation of Intrinsically Stretchable Organic Light-Emitting Diodes", ***Advanced Functional Materials*** (under revision)

Conference Presentations

1. **S. J. Han**, H. Zhou, S.-J. Kwon, T. -W. Lee, "Stretchable Graphene/Silver Nanowire Electrodes with High Work Function", *2019 International Meeting on Information Display*, August 27-30, Gyeongju, Korea (Poster presentation)

2. **S. J. Han**, H. Zhou, T.-W. Lee, "Work Function Tunable Intrinsically Stretchable Silver Nanowire/Graphene Electrodes based Passive Matrix Organic Light-Emitting Diodes", *2021 12th International Conference on Advanced Materials and Devices*, Dec. 6-10, Jeju (Poster presentation)